Renewable and Sustainable Energy Reviews 14 (2010) 2315–2338

Contents lists available at ScienceDirect

Renewable and Sustainable Energy Reviews

journal homepage: www.elsevier.com/locate/rser

A review of solar chimney power technology

Xinping Zhou [a,b,*], Fang Wang [a,b], Reccab M. Ochieng [c]

[a] Department of Mechanics, School of Civil Engineering and Mechanics, Huazhong University of Science and Technology, Luoyu Road 1037, Wuhan, Hubei 430074, PR China
[b] Hubei Key Laboratory for Engineering Structural Analysis and Safety Assessment, Huazhong University of Science and Technology, Luoyu Road 1037, Wuhan, Hubei 430074, PR China
[c] Department of Physics and Materials Science, Maseno University, P.O. Box 333, Maseno, Kenya

ARTICLE INFO

Article history:
Received 1 April 2010
Accepted 20 April 2010

Keywords:
Solar chimney
Solar collector
Turbine
Power conversion unit
Power generation

ABSTRACT

Utilization of solar chimney (SC) for power generation has proved to be a promising approach for future applications. This paper provides a comprehensive picture of research and development of SC power technology in the past few decades. The description, physical process, experimental and theoretical study status, and economics for the conventional SC power technology are included as well as descriptions of other types of SC power technology.

Contents

1. Introduction . . . 2316
2. Description . . . 2316
   2.1. Solar collector . . . 2317
   2.2. PCU . . . 2318
   2.3. SC . . . 2320
3. Physical process . . . 2321
   3.1. Solar collector . . . 2322
   3.2. Solar chimney (tower) . . . 2322
   3.3. PCU and power output . . . 2324
      3.3.1. Pressure drop at the turbine . . . 2324
      3.3.2. PCU efficiency . . . 2324
   3.4. Outflow from SC into atmosphere . . . 2327
4. Study status . . . 2327
   4.1. Experiment studies . . . 2327
   4.2. Theoretical studies . . . 2330
5. Economics . . . 2332
   5.1. Economics for power generation . . . 2332
   5.2. Additional revenues . . . 2332
6. Other types of SC power technology . . . 2333
   6.1. Floating SC power technology . . . 2333
   6.2. SC power technology with sloped collector . . . 2333
   6.3. SC power technology with mountain hollow . . . 2334
   6.4. SC power technology for harvesting atmospheric water . . . 2334
   6.5. Other combined SC power technologies . . . 2336
7. Discussions and conclusions . . . 2336
   Acknowledgements . . . 2336
   References . . . 2336

* Corresponding author.
E-mail address: xpzhou08@mail.hust.edu.cn (X. Zhou).

1364-0321/$ – see front matter
doi:10.1016/j.rser.2010.04.018

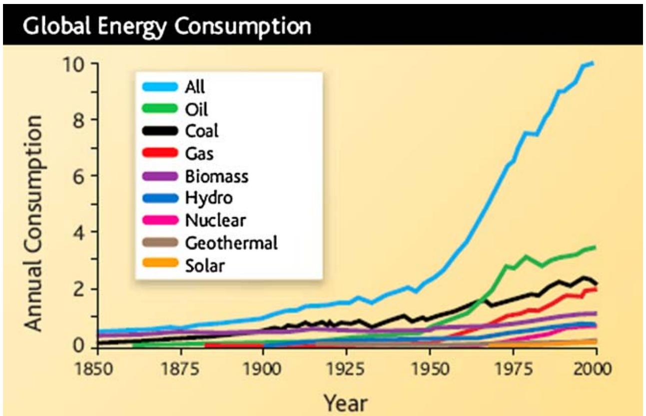


Fig. 1. Annual global energy consumption during the time between 1850 and 2000 [1].

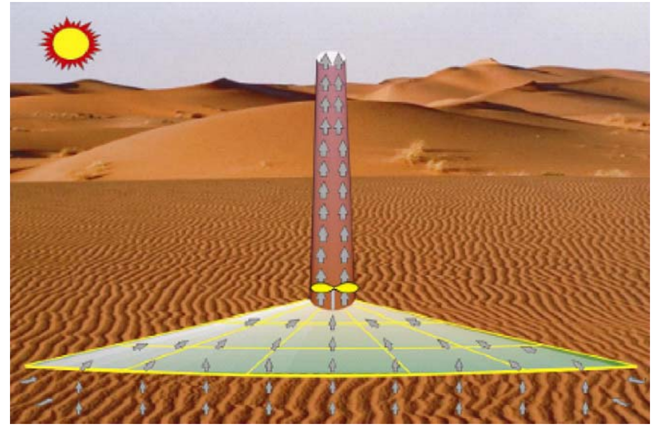


Fig. 3. Schematic diagram of SCPP.

1. Introduction

In recent years, rapid developments of global economy and increase in population and living standards have been posing great pressure on natural resources (Fig. 1 [1]) and the environment. Fossil fuels are being exhausted at a fast rate, and utilization of fossil fuels together with net deforestation [2] has induced considerable climate change in warming the atmosphere by releasing greenhouse gases (GHG) which may produce many negative effects including receding of glaciers, rise in sea level, loss of biodiversity, extinction of animals, and loss of productive forests [2], acidification of oceans, killing of heat waves, and retreat of butterflies up mountainsides worldwide [3]. The effect of glacier receding is one of the most notable effects. The satellite monitoring of Arctic sea ice area remaining in September of every year (the low point in a year) began in 1979 and showed the overall Arctic sea ice area shrank to the extreme record low minimum observed in September 2007 (Fig. 2) [4]. These effects have compromised the ability of many countries to develop sustainably [5]. Renewable energy sources can play a great role in solving the above problems in the future. SC power technology is a promising large-scale power technology [6–9], which absorbs direct and diffused solar radiation and converts parts of solar energy into electric power free of GHG emissions.

The solar chimney power plant (SCPP) combines three familiar components: a solar collector, a SC situated in the center of the collector, and power conversion unit (PCU) which includes one or several turbine generators. The turbines are driven by airflow produced by buoyancy resulting from greenhouse effect inside the collector (Fig. 3). This technology has been verified by the successful construction and operation of the 50 kW Manzanares SCPP prototype. The most suitable construction sites of large-scale SCPPs are located in vast desert regions where land may be free

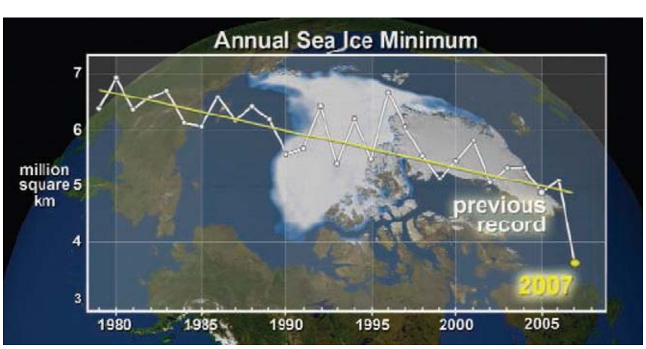


Fig. 2. Arctic sea ice area during time between 1979 and 2007 [4].

[10]. The technologies for the SCPP components are simple and reliable, accessible to the technologically less developed countries, which are sunny and often have limited raw material resources. Little maintenance and no combustible fuel and cooling water are needed for SCPPs. A major problem of SCPP is its low conversion efficiency as determined by the thermal performance of the system. However, the conversion efficiency of SCPP increases with the SC height. For commercial power plants producing energy economically, not only is a large collector area necessary for collecting solar energy, but also a high gigantic SC is required to obtain a large driving force and to produce a large volumetric flow to drive big turbines. Furthermore, a higher conversion efficiency for large-scale SCPP will also lead to a certain reduction in the energy cost.

In this paper, the details of SC power technology are described, and the status and development of this technology reviewed, including the physical processes, experimental and theoretical study status, and economics for this SC power technology. In addition the descriptions of other types of SC power technology are given.

2. Description

The SC power technology was first proposed by Cabanyes [11], and then described in a publication by Günter [12]. Several patents had been granted to Lucier in Australia, Canada, Israel and the USA since 1975 [13]. Schlaich again presented the technology in a congress in 1978 [14], and then together with his colleagues designed and constructed the first SCPP prototype in Manzanares, Spain during the two-year period between 1981 and 1982 [15–18]. This prototype had a SC 194.6 m high, a collector 122 m in radius, and a single vertical axis single-rotor turbine configuration with four blades installed at the SC base. This prototype operated with the peak power lying at about 50 kW for eight years [6,19], which verified the feasibility of this SC power technology. Since then, many researchers have shown strong interest in and extensively studied the huge-potential SC power technology all over the world. Some large-scale SCPP projects have been proposed in several countries. The Australia government decided to support the construction of a 200 MW SCPP in Mildura, Australia. The SC proposed in Australia has a SC 1000 m high and a collector 7000 m in diameter. This plant will provide enough electricity to power around 200,000 households, similar to the number of homes in Hobart, the capital of Tasmania, and reduce the emissions of annual greenhouse CO_2 gases of more than 900,000 tonnes [20]. A 40 MW SCPP called Ciudad Real Torre Solar was proposed to be constructed in Ciudad Real, Spain. This plant is programmed to include a SC 750 m high and a 3.5 km^2 collector [21]. In mid 2008,

the Namibian government approved a proposal for the construction of a 400 MW SCPP called ‘Greentower’ with a SC 1500 m high and 280 m in diameter, and a 37 km^2 collector. The collector is planned to be used additionally for agriculture as a greenhouse in which cash crops can be grown [22]. A proposal of building 1000 m high SC for power generation and tourism development in Shanghai, China was presented and its simulation requested was performed by HUST team.

In the past decades, different configurations or layouts for the SCPP components, i.e., collector, SC, and PCU, have been presented and investigated in order to improve the SCPP performance and its economics. The operation principle and different configurations and layouts of the SCPP components are reviewed in the next section.

2.1. Solar collector

Solar collector consists of support matrix, column structure, and transparent roof. A large air collector is formed, when a transparent glass or plastic roof supported above the ground by column structure and support matrix is stretched out horizontally many meters (Figs. 3 and 4). The height of the roof slowly increases along a radius from the periphery to the center to guide inward airflow with minimum friction losses. This transparent roof admits direct and diffused solar beam to be transmitted and retains long-wave radiation from the heated ground. Greenhouse effect is therefore produced in the collector. The ground under the roof heats up and transfers its heat to the air above it flowing radially from the periphery to the center driven by buoyancy.

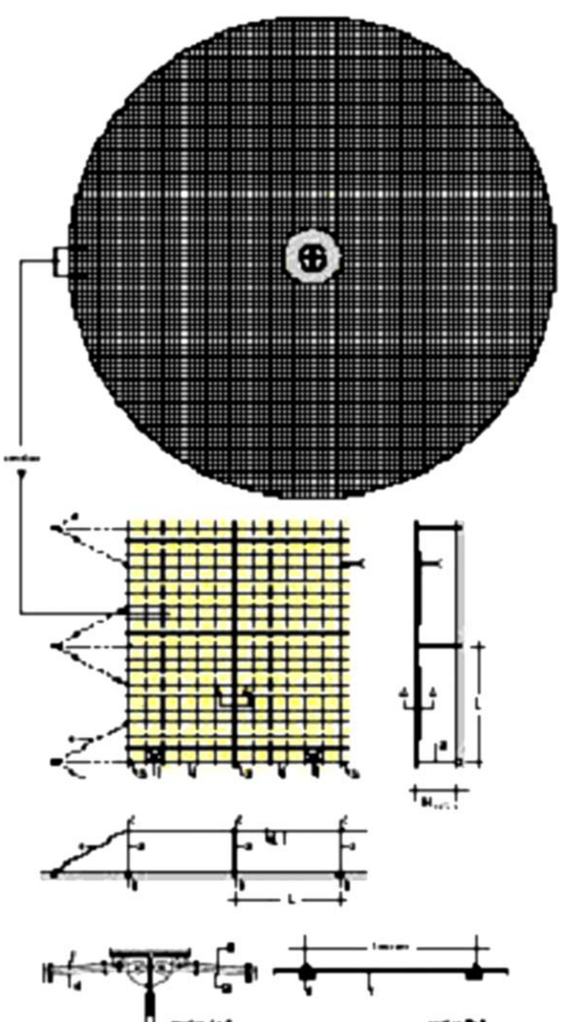


Fig. 4. Solar collector structure [6].

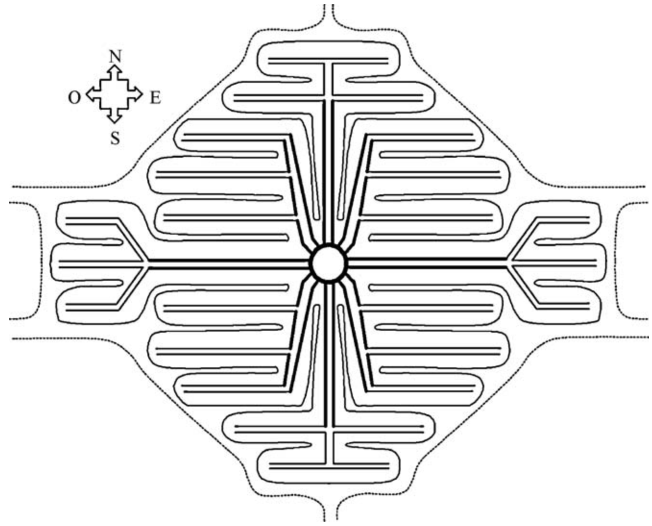


Fig. 5. Irregular solar collector configuration [23].

In order to reduce the turbulent friction losses effectively, a new collector concept with ribs containing their branchings was proposed by Bonnelle (Fig. 5) [23]. Compared with the conventional collector, this new design has larger entrance area compared to a circle with the same area. This leads to smaller air velocity, thus turbulent friction losses. Accordingly, the roof will be lowered and then the construction cost reduced.

Usually, natural soil has a certain thermal storage capacity, but its thermal storage capacity cannot meet the need of SCPP operation during night time. In order to improve the operational performance of SCPP during night time, some measures were proposed, mainly including to introduce an intermediate secondary roof under the first roof [24], to lay down an additional thermal storage system such as closed water-filled tanks (or tubes or bags) on the natural soil under the collector roof [25,26], and to use solar ponds for thermal storage of SCPP [27]. The introduced secondary roof divides the collector into a top and bottom sections, as shown in Fig. 6a [24]. An airflow regulating mechanism at the bottom section outlet is introduced to control the mass flow through the bottom section of the collector. Air flow through the bottom section is effectively controlled by incrementally increasing or decreasing the pressure drop across the regulating mechanism. This gives the plant the ability to store and release energy from the ground to regulate the power output of the plant. When less power is required, the bottom section is closed and energy is stored in the ground. Otherwise, the bottom section is opened in a controlled manner, producing an air flow under the secondary roof and releasing the energy stored in the ground. Thermal storage with water works more efficiently than with soil alone, since the specific heat capacity of water is much larger than that of soil and even at low water velocity – from natural convection in the tanks – the heat transfer between water tanks and water is much more efficient than that between ground surface and the soil layers underneath [25,26]. The tanks (Fig. 6b) filled with water remains closed, where no evaporation can take place. The upper surface of the tank is transparent to let solar beam be transmitted and the lower surface is painted black to absorb solar radiation effectively. During day time, some of the heat is stored in the additional water-filled thermal storage system but during night time, when the air in

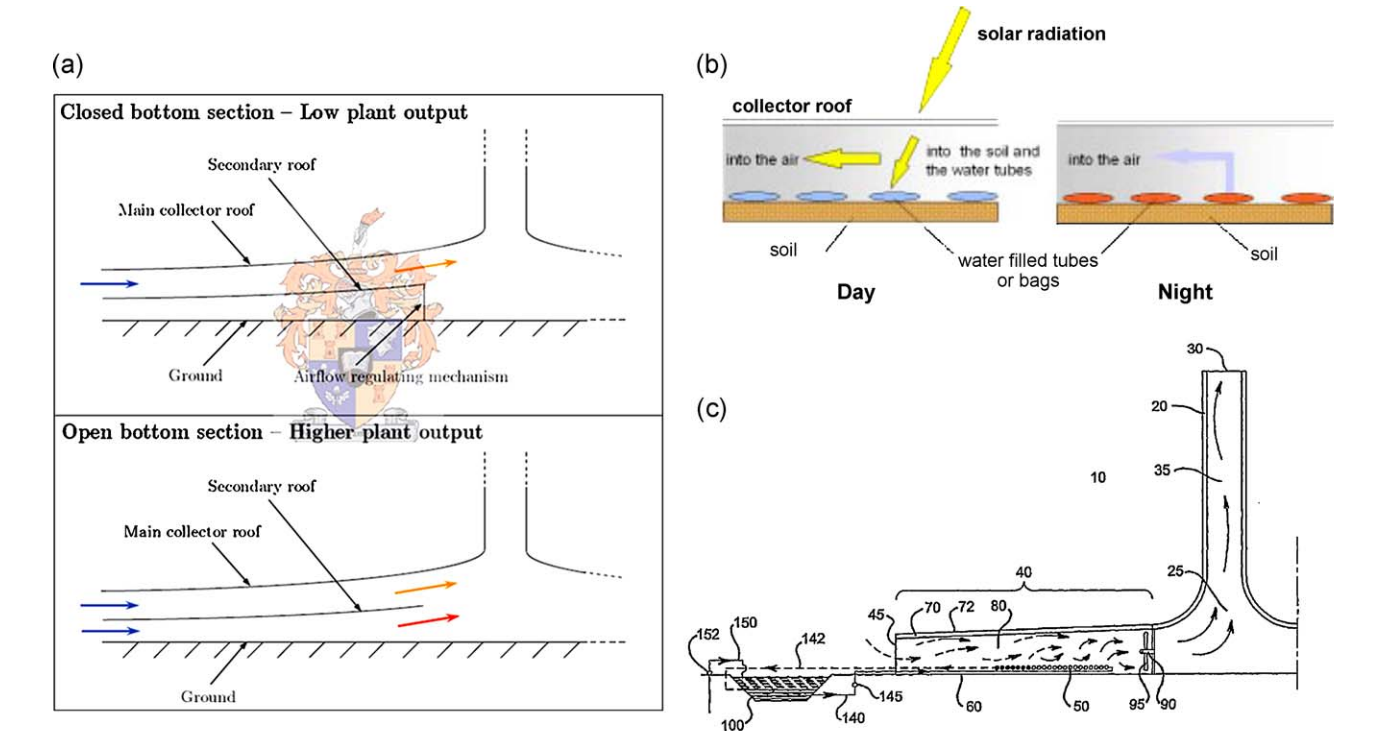


Fig. 6. Controlling SCPP's power output profile: (a) by introducing a secondary roof [24]; (b) by laying closed water-filled thermal storage system down on natural soil [26]; (c) by using solar pond for thermal storage [27]: 35: SC; 40: solar collector; 50: heat exchanger; 90: turbine; 100: solar ponds.

the collector starts to cool down, the water inside the tanks releases the heat stored during day time. The volume of water in the tank corresponding to water layer thickness is selected according to the desired characteristics of power output profiles during the day and night. The concept of using solar ponds for thermal storage of SCPP was proposed by Davey (Fig. 6c) [27]. This concept was adopted in the programmed large-scale EnviroMission's SCPP [7,28]. In this combined power system, hot brine is extracted from the lower convective zone, i.e., the thermal storage layer of solar ponds, to the heat exchanger to heat dry operating air in the collector, driving turbine generators to produce power during night time and cloudy day. This ensures consistent operation of SCPP with much more uniform power output profile day and night.

2.2. PCU

PCU of a large-scale SCPP consists of one or several turbine generators, power electronics, a grid interface and a horizontal-to-vertical transition section (HTVTS), i.e., the flow passage from collector exit to SC inlet. This transition section containing the turbine inlet guide vanes (IGV) redirects the flow from horizontal to vertical, and guides the flow through the turbine that powers a generator. A diffuser is possibly placed behind the turbines in the SC. Without doubt, this complex HTVTS configuration will induce the pressure losses.

Five possible geometric configurations for HTVTS (i.e., straight junction, curved junction, slanted junction, conic SC, and curved junction with guiding cone) based on the three basic geometric configurations (Fig. 7) were presented and compared by Bernardes et al. [29] from a mass flow (Table 1) and recirculation point of view by simulating thermodynamic behavior in SCPPs with different HTVTS configurations using a model of natural laminar convection.

Geometric configurations of HTVTS can induce perturbations (recirculations) of flow which is reflected on the aerodynamic behavior. Bernardes et al.'s study showed that the mass flow and the collector air temperature rise were the highest for a conic SC as expected. This conclusion is also consistent with Yan et al.'s study [30]. While, the air mass flow $\dot{m}_f$ for a straight junction is the smallest, because flow recirculations appear at the junction. Higher flow is produced when a curved junction is used. The introduction of a guiding cone in the center did not bring major thermodynamic improvements. Müller [31] found that such a guiding cone in the collector center can reduce losses by 43% for the SCPP with multiple horizontal axis turbine configurations.

The turbine generators are core components of any SCPP. The main function of the SC turbine is the efficient conversion of fluid power to shaft power. The typical SC turbine is of the axial flow type. Its characteristics (e.g., the number of rotor blades, specific

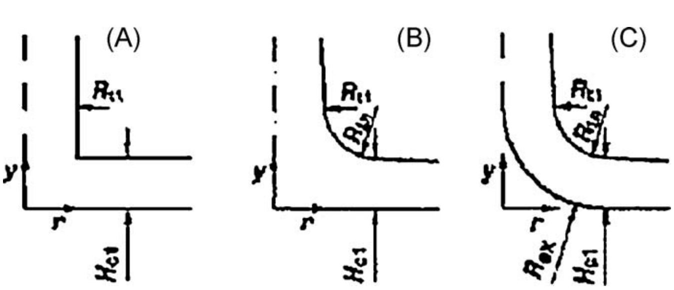


Fig. 7. Basic geometric configurations for HTVTS [29].

Table 1
Mass flow rate of different geometric configurations for HTVTS [29].

Case	H_{c1}	R_{t1}	R_{in}	R_{ex}	$\dot{m}_f$ (kg/s)
Straight junction	0.02	0.05	–	–	8.31×10^{-4}
Curved junction	0.02	0.05	0.1	–	1.08×10^{-3}
Slanted junction	0.07	0.05	0.1	–	1.29×10^{-3}
Conic SC	0.02	0.1	0.1	–	1.92×10^{-3}
Curved junction with guiding cone	0.02	0.05	0.1	0.12	1.1×10^{-3}

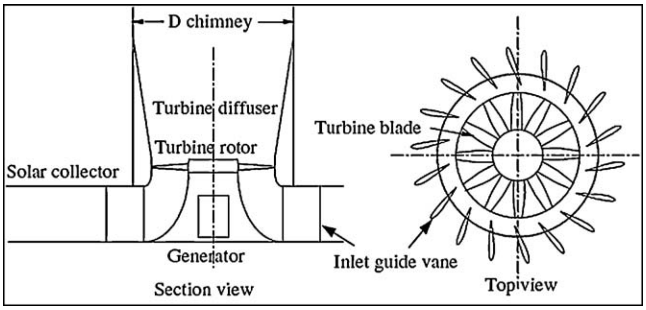


Fig. 8. SC SVSTa layout [32].

speed of blades, and turbine diameter) lie between those of wind turbine and gas turbine. Its blades are adjustable like those of wind turbine, but as in gas turbine the flow is enclosed, and the SC turbine may have radial inflow IGVs (Fig. 8) [32–34].

Various installation locations, configurations and layouts have been proposed for the SC turbines. The conventional SC turbines are usually placed at the SC base [6]. Pasumarthi and Sherif [14] proposed turbines to be installed at the SC top. Bonnelle [23] compared the static pressure fields of airflow in SCs where the turbines were respectively placed at the base and the top. Relative negative pressure appeared in the SC when the turbine was placed at the SC base, while relative positive pressure appeared when the turbine was placed at the SC top. These depend on the fact that static pressure must drop largely from the upstream to downstream of a turbine. In most literature about SCPP, the SC turbines were proposed to be placed at the SC base mainly because of inconvenience arising from installation and maintenance of turbine generators at the SC top for large-scale SCPP.

Schlaich presented three possible turbine configurations including the single vertical axis, the multiple vertical axis and the multiple horizontal axis turbine configurations (Fig. 9) [6,35,36]. Various layouts were proposed for the SC turbines. Schwarz and Knauss [37] designed a single vertical-axis single-rotor turbine without IGV for the Manzanares plant. Gannon and von Backström [32–34] proposed a single vertical-axis single-rotor turbine for a large-scale SCPP where the SC support structures are used as IGVs (Fig. 8). They presented an analytical model for this layout, which is adapted from gas turbine literature, and showed that IGV improved the performance of SC turbine. Denantes and Bilgen [38] introduced an alternative turbine layout consisting of one pair of counter-rotating rotors, either with or without IGV. The schematic diagram of the four turbine layouts can be presented in Fig. 10, including single-rotor and counter-rotating turbines, both with or without IGV [39]. Therefore, six turbine types can be considered as below:

(1) The single vertical-axis single-rotor turbine with or without IGV (SVST(a or b)).
(2) The single vertical-axis counter-rotating turbine with or without IGV (SVCT(a or b)).
(3) The multiple vertical-axis single-rotor turbine with or without IGV (MVST(a or b)).

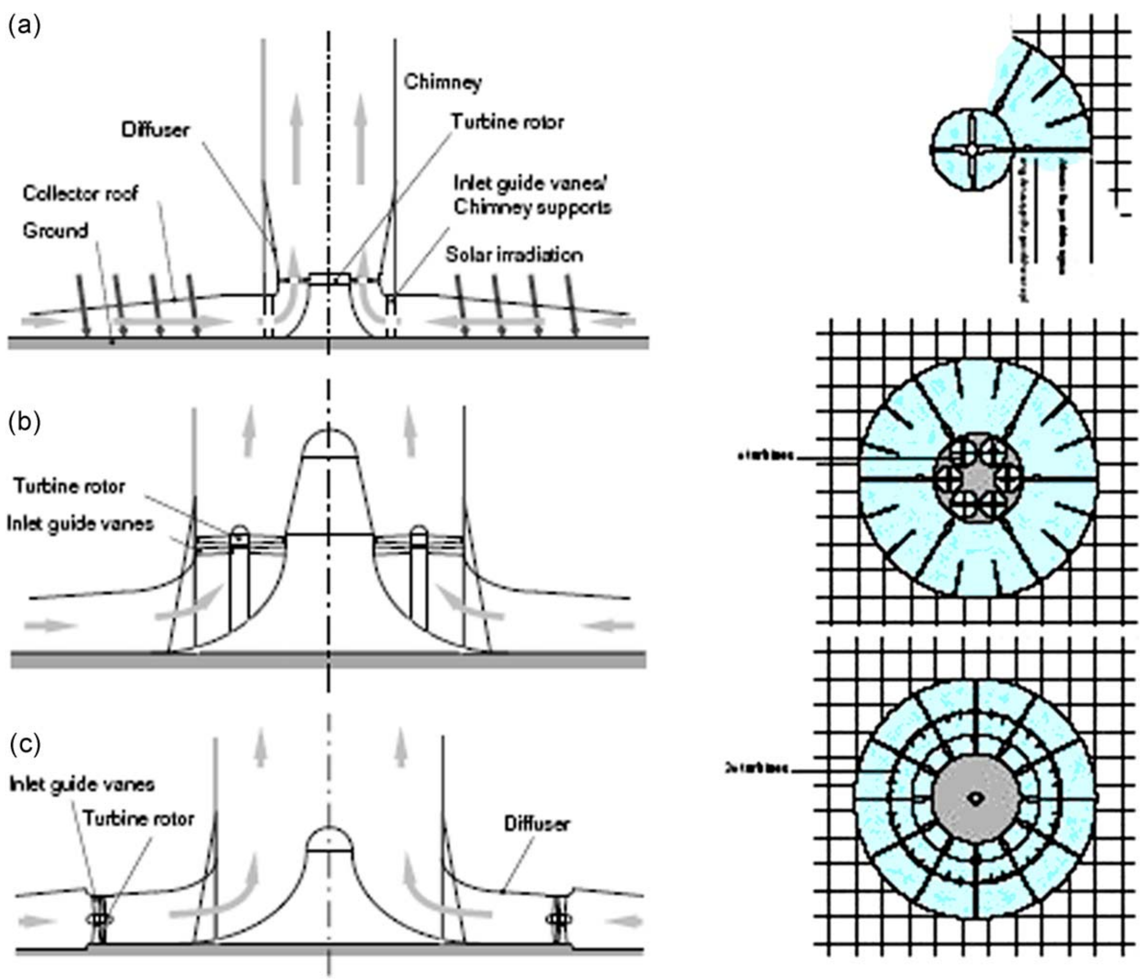


Fig. 9. Vertical view and top view of three turbine configurations: (a) single vertical axis type; (b) multiple vertical axis type; (c) multiple horizontal axis type [6,36].

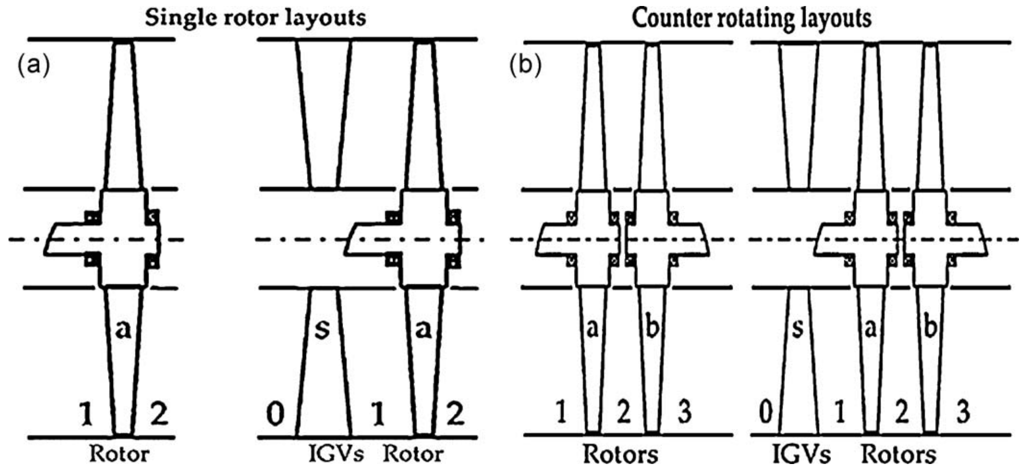


Fig. 10. Schematic diagram of turbine layouts including single rotor and counter rotating turbines, both with or without IGVs [39].

(4) The multiple vertical-axis counter-rotating turbine with or without IGV (MVCT(a or b)).
(5) The multiple horizontal-axis single-rotor turbine with or without IGV (MHST(a or b)).
(6) The multiple horizontal-axis counter-rotating turbine with or without IGV (MHCT(a or b)).

2.3. SC

The SC situated in the collector center is the actual thermal engine of the SCPP, which drives the air to flow in the collector to the SC base by combining with the effect of temperature difference. It is a pressure tube with low friction losses because of its favorable surface–volume ratio. The mass flow of the updraft air is approximately proportional to the collector air temperature rise and to the SC height.

The structure design and construction of the high, gigantic SC for commercial SCPP is an important thing. Schlaich [6,40] thought that the best choice for high SC structure is reinforced concrete structure because of the longest life-span at the most favorable costs among the many possible construction methods and the materials of building SC, e.g., covered steel framework with cable nets, membranes, trapezoidal metal sheet, etc., although they designed a guyed corrugated metal sheet flue for SC in the Manzanares plant prototype just for experimental measurements. Later, they designed a serial of reinforced concrete cylindrical SCs for commercial SCPPs. The highest height of these SCs reached was 1000 m [6,26,40]. Schlaich [40] designed the structure of a gigantic

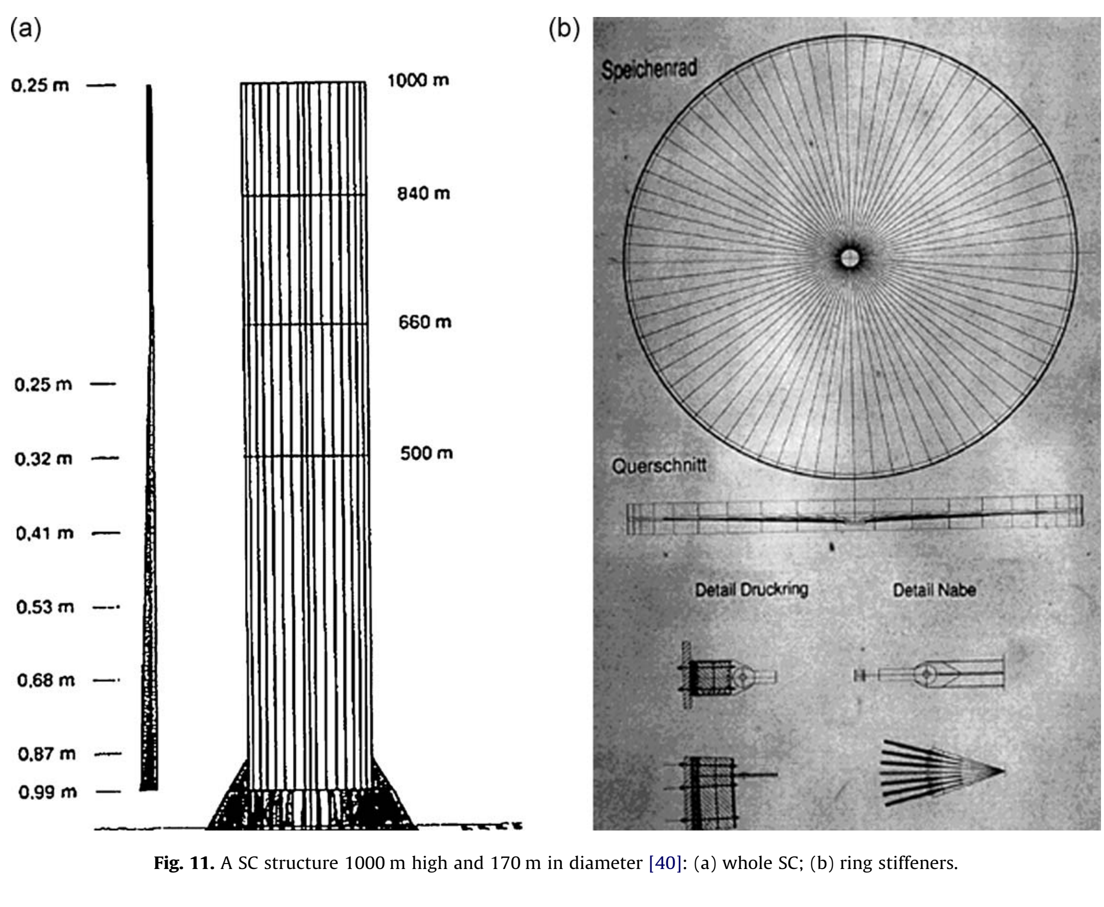


Fig. 11. A SC structure 1000 m high and 170 m in diameter [40]: (a) whole SC; (b) ring stiffeners.

1000 m-height and 170 m-outer diameter SC case (Fig. 11). The shell thickness decreases from 0.99 m just above the support on radial walls to 0.25 m halfway up, then remaining constant all the way to the top. The compression ring stiffeners are installed with a vertical spacing to support the high, gigantic SC structure [40]. The ring stiffeners in the SC have to serve two mechanical duties, i.e., to force the cross sections from shell-like deformations to beam-like ones, and to increase the buckling stiffness of the SC structure. The meridional stresses in the reference SC wall can be reduced to an extent that tension disappears completely with use of ring stiffeners (Fig. 12).

Gannon [33] presented a 200 MW plant where SC height and diameter reached striking values of 1500 and 160 m respectively, and designed the thickness of the reinforced concrete shell ranging from 2.19 to 0.25 m for a 1500 m high SC, whereas Harte and Van Zijl [41] designed shell thickness gradually changing from 2 m at the base to 0.25 m at 1000 m height and then remaining constant all the way to the top. Majority of the Gannon's and his coworkers' work [32–34,42–45] was based on the SC 1500 m high and 160 m in diameter [30].

A twin-shell concept (Fig. 13) was proposed by Sawka [46] for SC structure to improve its stiffness and dynamic stability. A hyperbolic concrete shell was added to the lower part of the cylindrical shell and the SC outlet was opened by a bellmouth shape. This conceptual structure would fit better to multiple horizontal axis turbines. Its horizontal deflections will be reduced, and its eigenfrequencies will be enhanced to be more sufficiently against resonant excitations exposed to environmental wind.

Based on the experiences of concrete cooling towers especially at the Niederaussem concrete cooling tower 200 m high (which has been the highest cooling tower in the world at the moment) [47], Krätzig and coworkers [48,49] designed a serial of hyperbolic SCs with heights ranging from 500 to 1500 m. Taking a 1000 m high SC of a 200 MW SCPP for an example, the SC structure was designed and shown in Fig. 14 [49]. The predominant parts of the shell will be constructed using high-performance concrete C 70/85, whose compression strength is comparable to (low quality) cast iron. In order to control possible cracking on the outer surface of shell, the concrete may be modified in the sense of a unilateral stress–strain-behavior, to reduce its tension strength to the level of concrete C 30/37.

In the upper two thirds the SC shell is formed as a conical frustrum in upside-down position resulting from aerodynamics aspects. It is stiffened by compression rings with a vertical spacing of 100 m which may be additionally pre-stressed by spoke wheels fabricated of strings from carbon fiber resin. The spokes were supported to be made of vertical steel slats in the Schlaich's design [40]. The spokes are directed in such a manner (Fig. 14) that their mechanical effects reach at maximum values. The manner differs from the Schlaich's design (Fig. 11a) [40]. In the lower one third the SC shell applies the benefits of strengthening of shell structure: The shear stresses can be minimized by using a hyperboloidal meridional curve. This leads to mainly meridional stresses in the narrow residuals of the SC shell between the turbine openings, thus simplifying the SC foundation considerably [49].

Generally speaking, the optimum shaping and ring-stiffening of SC should be determined to allow an economical construction by using conventional climbing systems, and to guarantee long durability for the designed service life of at least 80 years [6,49].

3. Physical process

The air cycle with losses for SCPP is shown in Fig. 15 [42] where 02–03 process denotes the air entering from the collector inlet is heated by insolation when its temperature and entropy increase; 03–3te process denotes the air at the collector outlet blows through the turbine when the temperature decreases slightly; 03te–04 process denotes the air behind the turbine flows through the SC when the temperature decreases due to the negative work of gravitational force. Finally, the energy including dynamic energy and thermal energy of airflow is released into the atmosphere. The losses through the power system are also included in this cycle. The aerodynamic losses of PCU components are respectively included in the collector and in the SC except turbine losses, as shown in Fig. 15.

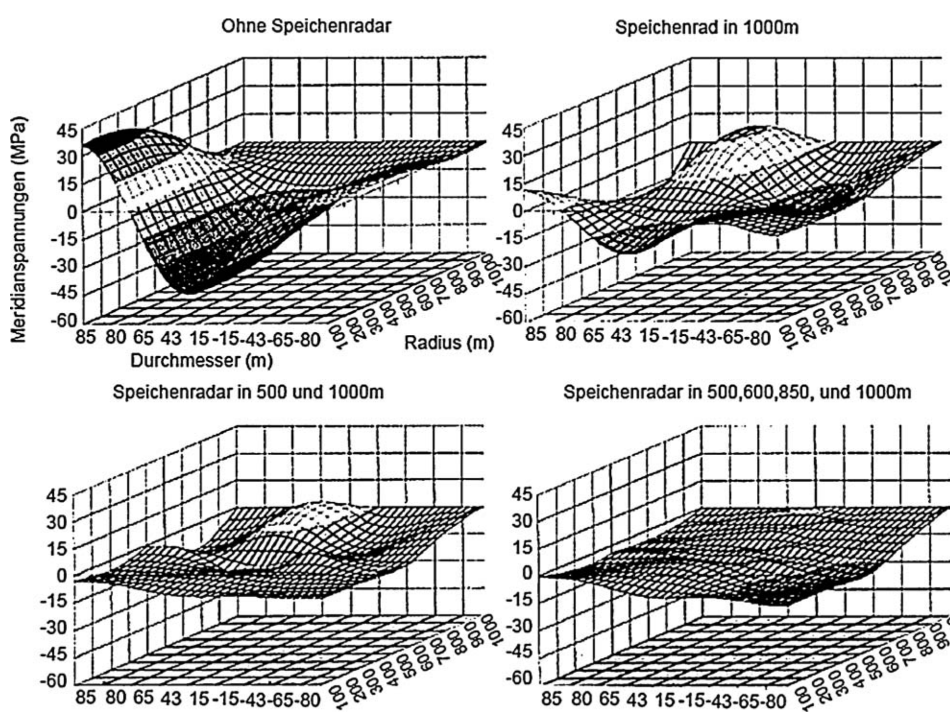


Fig. 12. Meridional stresses in the reference SC wall around its periphery and along its height depending on the number of stiffening spoked wheels [40].

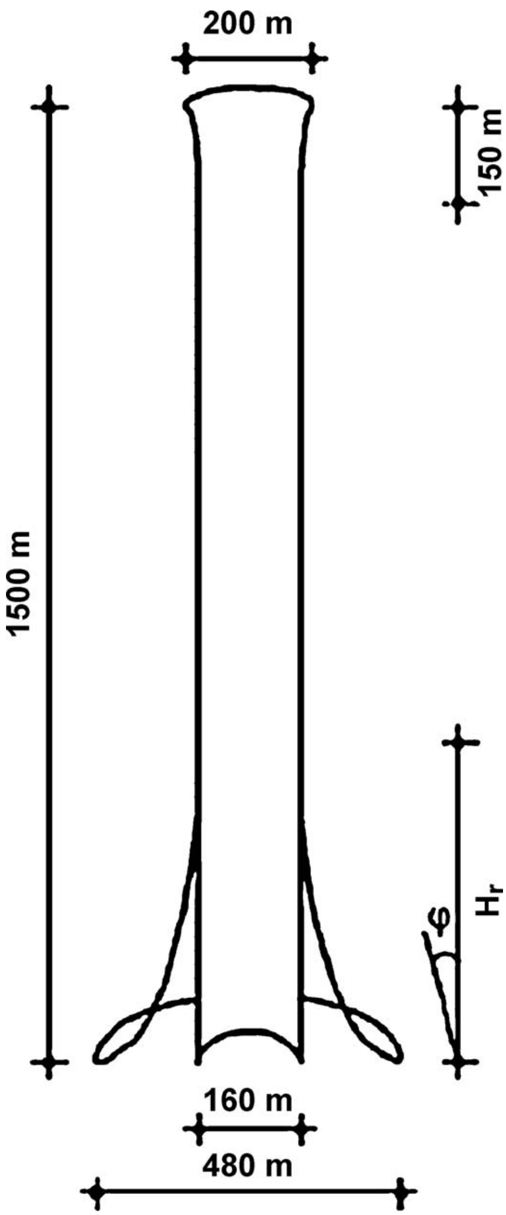


Fig. 13. Schematic diagram of twin-shell SCPP [46].

3.1. Solar collector

The heat transfer and air flow can be simulated by solving the relevant conservation equations. Pretorius [24,50–52] presented the comprehensive equations for an elementary control volume in the system. Since the changes of the air dynamics are relatively slow along a radius, transient terms in the conservation equations are negligible [50,53]. The relevant equations are:

Continuity

$$\frac{\partial}{\partial r}(\rho v r h) = 0 \tag{1}$$

Momentum

$$\rho v h \frac{\partial v}{\partial r} = -h \frac{\partial p}{\partial r} - \tau \tag{2}$$

where τ is the shear stress item, which should include effect of friction on the ground surface and the roof and the drag exerted by the supports. The expression of τ is given by Pretorius [24,51], and leads to the aerodynamic losses in the collector.

Collector air energy is represented by

$$q_{rh} + q_{gh} = \frac{0.4 c_v T}{r} \frac{\partial}{\partial r}(\rho v r h) + \rho v h \frac{\partial}{\partial r}(c_p T) \tag{3}$$

whereas the roof energy and ground energy equations are respectively written as

$$\alpha_{eb} I_{hb} + \alpha_{ed} I_{hd} + q_{gr} = q_{ra} + q_{rs} + q_{rh} \tag{4}$$

and

$$(\tau_e \alpha_g)_b I_{hb} + (\tau_e \alpha_g)_d I_{hd} = q_{gr} - k_g \frac{\partial T_g}{\partial z}\bigg|_{z=0} + q_{gh} \tag{5}$$

By assuming constant ground properties, the energy balance below the ground surface is mathematically expressed as

$$-k_g \frac{\partial^2 T_g}{\partial z^2} + \rho_g c_{pg} \frac{\partial T_g}{\partial z} = 0 \tag{6}$$

with a boundary condition at a considerable depth

$$\frac{\partial T_g}{\partial z} = 0 \tag{7}$$

Bernardes et al. [54,55], and Pretorius et al. [24,51,56] performed the comprehensive studies on heat transfer and air flow in SCPP. The empirical equations were presented for heat transfer coefficients from roof to operational air, from roof to the ambient, from ground to operational air in their papers. Bernardes et al. [57,58] compared the methods used to calculate the heat fluxes in the collector, and their effects on SCPP performance. In general, the Pretorius model produces higher heat transfer coefficients and higher heat fluxes both for the roof and for the ground surface. The results showed that the values of air temperature rise and power output calculated using the two methods were similar.

3.2. Solar chimney (tower)

The pressure potential, i.e., the pressure difference between the SC inward air and the ambient air, is the driving force potential of airflow. It can be given by [6]

$$\Delta p_{tot} = g \int_0^{H_{ch}} (\rho_\infty - \rho) dh \tag{8}$$

By assuming a dry adiabatic lapse rate for the air inside and outside the SC and location of turbine at the ground level, the pressure potential can be further expressed as [59]

$$\Delta p_{tot} = p_{\infty 0}\left(1 - \frac{1 - gH_{ch}/(c_p T_{\infty 0})}{1 - gH_{ch}/(c_p T_{te})}\right)^{\gamma/(\gamma-1)} \tag{9}$$

Relevant conservation equations for continuity, momentum, and air energy are derived for an elementary control volume in the SC [51]. These equations are

Continuity

$$\frac{\partial}{\partial z}(\rho w) = 0 \tag{10}$$

Momentum

$$\rho w \frac{\partial w}{\partial z} = -\frac{\partial p}{\partial z} - \frac{4\tau_{ch}}{D_{ch}} - \rho g \tag{11}$$

SC air energy

$$0.4 c_v T \frac{\partial}{\partial z}(\rho w) + \rho w \frac{\partial}{\partial z}(c_p T) + \frac{\partial}{\partial z}(\rho g w z) = 0 \tag{12}$$

von Backström and Gannon [45] firstly presented that the flow through SC should be considered to be a compressible flow because the change in density due to change in altitude plays a role in

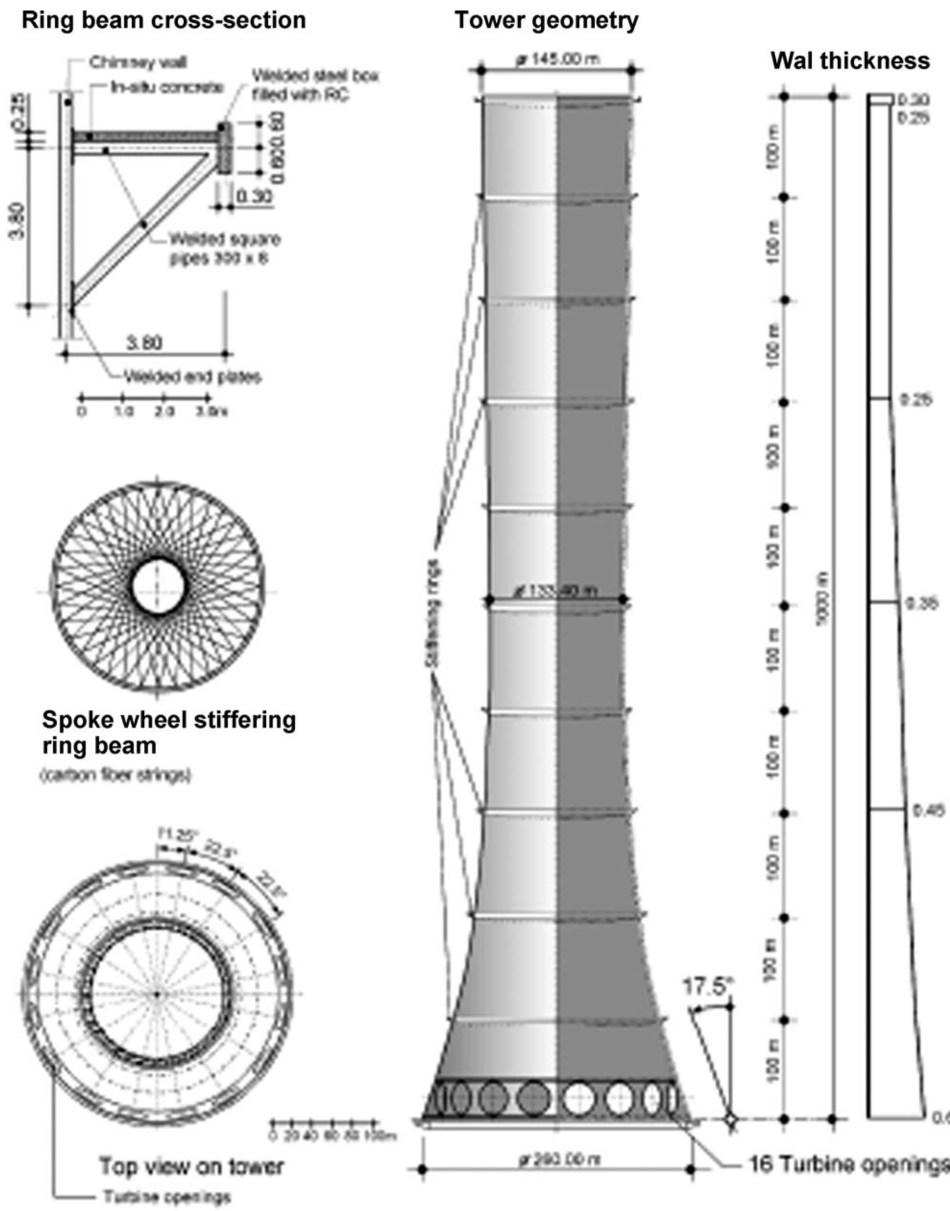


Fig. 14. A 1000 m high SC structure [49].

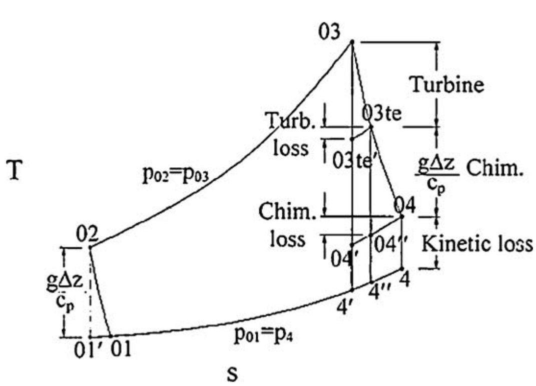


Fig. 15. Temperature–entropy diagram of air standard cycle analysis with system losses [42]: 01: atmospheric air at SC outlet; 02: collector inlet air; 03: collector outlet air; 04: SC outlet air.

buoyancy (i.e., driving force of airflow) in a super-high SC, and they theoretically deduced the relational expressions of the performances of air at the SC outlet and inlet by assuming the internal drag, work and heat inputs to be equal to 0 behind the diffuser (or turbine without diffuser) in a constant sectional area SC. Zhou et al. [60] compared the model of compressible flow through SC to Boussinesq model and full-buoyancy model with the help of computational fluid dynamics (CFD) software Fluent [61]. The Boussinesq model considers an incompressible flow, where the density is treated as a constant parameter and the Boussinesq approximation to the variation of local density is employed with the source term in the momentum equation [61,62]. In the full-buoyancy model, buoyancy reference density is kept constant, while the flow in computational domain is treated as compressible flow with its density being variable, and full buoyancy is implemented by adding a buoyancy force source term to the momentum equation [62]. The case study of the 1500 m high SC proposed by von Backström and Gannon [45] showed that the other two models gave 1.17 times and 1.14 times larger velocities of airflow at the SC inlet, and about 1.42 and 1.33 times more

power, respectively, than the compressible flow model [60]. The relational expressions of static pressure p, Mach number M, density ρ, and stagnation temperature ST for the compressible flow through SC are given by [45]

$$p = p_{ch,in}\left(1-\frac{g\cdot z}{c_p\cdot ST_{ch,in}}\right)^{\gamma/(\gamma-1)} \tag{13}$$

$$M = M_{ch,in}\left(1-\frac{g\cdot z}{c_p\cdot ST_{ch,in}}\right)^{-(\gamma+1)/(2(\gamma-1))} \tag{14}$$

$$\rho = \rho_{ch,in}\left(\frac{M_{ch,in}}{M}\right) \tag{15}$$

$$ST = ST_{ch,in} - \frac{g\cdot z}{c_p} \tag{16}$$

The SC losses are composed of many components, i.e., the wall friction loss, the loss resulting from the drag exerted by ring stiffeners, the exit kinetic energy loss, and additional vertical acceleration loss. von Backström and Gannon [45] estimated the coefficients of loss components for the reference SC 1500 m high. von Backström et al. [43] obtained two sets of loss coefficients from the measurements with non-swirling uniform inlet flow and with simulated swirling turbine exit flow in an experimental setup, respectively, and estimated the loss coefficients for the standard fully developed flow in the reference 1500 m high SC by considering the Reynolds number scale effect based on the measurements (Table 2).

3.3. PCU and power output

The power output from SCPP transmitted to grid interface [63,64] can be calculated by

$$P = \eta_{DT}\,\Delta p_{tur}\dot{V} = \eta_{DT}\eta_t\eta_L\,\Delta p_{tot}A_{ch}w_{ch,in} \tag{17}$$

where $w_{ch,in}$ is the velocity of air flow at the chimney inlet with turbine and diffuser installed, η_{DT} is the total mechanical and electrical efficiency, η_L is the aerodynamic efficiency obtained by considering the total aerodynamic losses in the system where the losses occurring in the collector and the SC have been summarized in Sections 3.1 and 3.2 and included in the momentum equations, and the losses in the PCU including many components are the most complex, while η_t is the factor of pressure drop at the turbine, which is the ratio of pressure drop at the turbine to pressure potential Δp_{tot} subtracting the pressure losses in the system. By assuming heat generated due to frictional losses is used to reheat airflow, the static pressure and temperature of air behind the PCU can be given by

$$\begin{aligned} p_{PCU} &= p_{\infty 0} - \Delta p_{coll} - \Delta p_{PCU} \\ &= p_{\infty 0} - \Delta p_{coll} - ((1-\eta_L)\Delta p_{tot} + \eta_t\eta_L\Delta p_{tot}) \end{aligned} \tag{18}$$

$$T_{PCU} = T_{coll,out} - \frac{\eta_t\eta_L\Delta p_{tot}A_{ch}w_{ch,in}}{c_p\dot{m}_f} \tag{19}$$

3.3.1. Pressure drop at the turbine

In reality, insolation has been changing with time. Even under constant insolation conditions, the pressure potential also changes with the rise in collector inward air temperature which changes with flow rate. Therefore, η_t always varies. In order to calculate the power taken up by the SC turbine conveniently, a constant value is always used in nearly all the literature about SCPP. Some researchers, e.g., Pasumarthi and Sherif [14], Pastohr et al. [65], Onyango and Ochieng [66], regarded the SC turbine as wind turbine and used the optimal η_t value at 16/27 based on the Betz limit of wind turbine. Some other researchers, e.g., Schlaich [6], Haaf et al. [15], Lautenschlaqer et al. [67], Mullett [63], von Backström and Gannon [69], Zhou et al. [68] used the optimum η_t value at 2/3, by assuming pressure potential to be a constant parameter and η_t to be independent of flow rate. Hedderwick [70] presented graphs which showed the values at around 0.7. Schlaich et al. [26] recommended a value of 0.8, whereas Bernardes et al. [55] reported that the mechanical power taken up by the turbine reached at maximum when η_t was equal to but hardly reached approximately 0.97 and therefore, recommended a value between 0.8 and 0.9 in reality, and used a value of 0.9 in their work. von Backström and Fluri [71] used an analytical approach to investigate the maximum fluid power condition in the collector, and reported the optimum η_t value of $(n-m)/(n+1)$, where m and n are pressure potential exponent and pressure loss exponent, respectively. The value of n will typically be equal to 2 when system pressure drop is dominated by minor losses and closer to 1.75 when the pressure drop is dominated by Reynolds number dependent wall friction losses [71,72]. m is typically a negative number between 0 and −1. The optimum η_t value is typically a number between 2/3 and 1, and is equal to 2/3 when pressure potential is assumed to be constant, i.e., $m = 0$. For the real large-scale SCPPs, the values of n are assumed to be equal to 2 for the system pressure potential abstracting the total pressure losses in the whole system, $\eta_L\,\Delta p_{tot}$, and the system losses are considered independently.

3.3.2. PCU efficiency

In most literature, PCU efficiency is just regarded as the efficiency of turbine generators by neglecting other component losses. In reality, the PCU losses can be divided into three parts, namely aerodynamic, mechanical and electrical losses. The aerodynamic losses would be treated in detail including intake losses, turbine losses, diffusion losses, mixing losses, and HTVTS losses, etc. The mechanical and electrical losses are summarized as drive train losses. The drive train includes all components necessary to convert the mechanical power delivered by the turbine rotors to electrical power ready for grid feeding, including gearbox, generators, power electronics and grid interface systems. In reality, in order to calculate the power taken up by the turbine conveniently, a constant value was used in nearly all the literature about SCPP, e.g., 83% reported by Haaf et al. [15], 40–80% by Mullett [63], 77, 78.3, and 80.1% respectively for 5, 30, and 100 MW SCPP by Schlaich [6] and Pasumarthi and Sherif [14], 80% by von

Table 2
Summary of coefficients of loss components in a reference SC 1500 m high [45,43].

Loss coefficient type	von Backström and Gannon [45]	Standard fully developed flow friction calculation and exit kinetic energy coefficient [43]	From measurement with non-swirling uniform inlet flow (sucked through) [43]	From measurement with simulated swirling turbine exit flow (blown through) [43]
Wall friction loss	0.008428	0.00846	0.01097	0.01367
Ring stiffener loss	0.25	0.0897	0.0897	0.122
Additional vertical acceleration loss	0.27	–	–	–
Exit kinetic energy loss	1.12	1.058	1.26	1.26

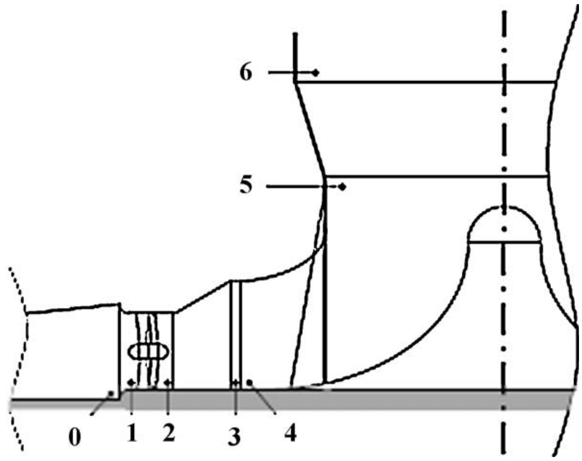


Fig. 16. Schematic diagram of SC PCU with multiple horizontal axis turbine configuration: 0: collector exit; 1: turbine inlet (after the bellmouth); 2: turbine exit; 3: exit of diffuser/nozzle directly after turbine; 4: exit of mixing section; 5: exit of HTVTS; 6: exit of diffuser section in SC [36].

Backström and Gannon [45] and Pretorius and Kröger [51], 75% by Bernardes et al. [55], and a potential value between 50% and 90% by Zhou et al. [66] for SVST. Fluri and von Backström [36] introduced an analytical model for each loss component in PCU. Taking a SC PCU with multiple horizontal axis turbine configuration for an example, Fig. 16 showed a schematic drawing of the SC PCU indicating the various locations in the flow passage. The design of the flow passage in an appropriate manner can let the aerodynamic losses to be low. The PCU aerodynamic loss components and drive train losses were reviewed as follows.

3.3.2.1. Intake losses. For the single vertical axis turbine configuration, no special intake is necessary, and the intake losses are included in the HTVTS loss model.

For the multiple horizontal axis turbine configuration, Kolb and Helmrich [73] proposed a rather bulky intake geometry with converging sections and a transition from rectangular to circular and analyzed it with CFD technology. Fluri and von Backström [36] proposed a circular bellmouth type intake which is much shorter than the geometry proposed by Kolb and Helmrich [73]. Inlet losses for this circular bellmouth type intake can be expected to be lower. A bellmouth provides a more uniform velocity profile, thus leading to a smaller dynamic load on turbine rotor blades, while its cost is not expected to be higher. Fluri and von Backström [36] estimated the intake loss coefficient using the Idelchik's expression about a wall-mounted bellmouth as

$$\zeta_{BM} = 0.5e^{-14.114(r/d_h)} \tag{20}$$

where r is the bellmouth radius, and d_h is the hydraulic diameter of the duct. Fluri and von Backström [36] used a value of 0.09 for intake loss coefficient by assuming the value of r/d_h to be 0.12.

For the multiple vertical axis turbine configuration, the same intake loss model was used. Although the geometry would look different, it is assumed to be good enough for a first approximation [36].

3.3.2.2. Turbine losses. In majority of mathematical models to predict the performance of SCPPs, one of the three PCU configurations, as shown in Fig. 9, was usually used without giving any reason. Kolb and Helmrich [73] compared SVST and MHST configuration for a 200 MW SCPP using CFD method. Denantes and Bilgen [38] compared the torque of SVCTa or SVCTb to SVSTa by modifying the von Backström and Gannon's analytical model for single-rotor turbine [32] to accommodate the layouts

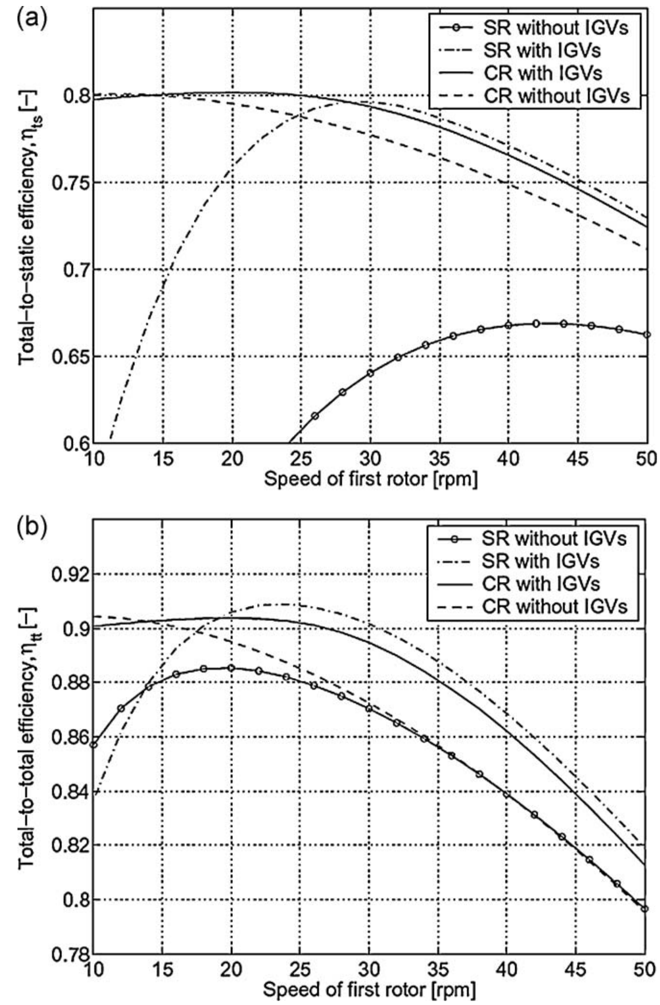


Fig. 17. Efficiency prediction for four turbine layouts for a single axial turbine configuration: (a) total-to-static efficiency; (b) total-to-total efficiency [39].

with counter-rotating rotors. They found that the single rotor layout had a higher efficiency at the design point but a lower efficiency at off-design conditions.

Fluri and von Backström [35,39] compared the performance of the four turbine layouts, including single-rotor and counter-rotating turbines, both with or without IGV using analytical models and discussed optimization techniques, and the important design parameters for the turbine layouts. In contrast to similar investigations found in literatures [32,38], various radial sections along the blades are analyzed by using the Fluri and von Backström's turbine model, which is more appropriate than using a simple mean line analysis when dealing with turbines with high blade aspect ratio and low hub to tip ratio. The predicted efficiency for the various turbine layouts for a single axial turbine configuration over a range of turbine speeds is shown in Fig. 17. Total-to-static efficiency of the single rotor layout without IGV is not satisfactory at any speed, with its peak lying at 66.9%. Either a stator or an additional rotor row is therefore required to be equipped. The peak total-to-static efficiencies of the other three layouts lie in a narrow band between 79.6 (SR with IGVs) and 80.1% (CR with IGVs). However, the speed of the first rotor at the peak efficiency differs largely for the three layouts. The single rotor turbine performs very poorly at low speeds, mainly due to high exit losses caused by a high exit swirl, which is necessary to prevent diffusion at the hub. It performs best at 29.2 rpm. With an increase in speed, the performance deteriorates mainly due to high rotor losses resulting from high relative flow velocity [39]. Based on the study on the above four turbine layouts

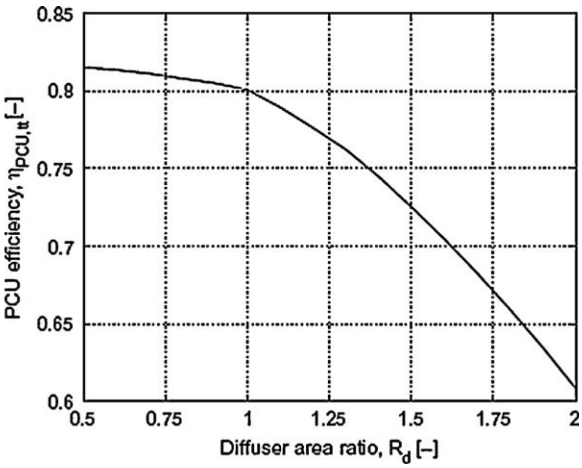


Fig. 18. Total-to-total efficiency of PCU versus diffuser area ratio for multiple horizontal turbine configuration [36].

[39], Fluri and von Backström [36] compared three turbine configurations (i.e., the single vertical axis, the multiple vertical axis and the multiple horizontal axis turbine configuration) from a SCPP's efficiency and energy yield point of view by calculating with a mathematical model.

3.3.2.3. Diffusion losses. For the multiple horizontal axis turbine configuration, there are two diffusions in the SC PCU respectively placed after the turbine rotors where the hub ends and in the actual diffuser (Fig. 16). The second is included in the turbine models [33,35,39], while the first was only considered by Fluri and von Backström [36]. von Backström and Gannon selected a value at 0.75 for the second diffuser efficiency when analyzing the turbine performance for a 200 MW SCPP case, whereas Fluri and von Backström [39] analyzed the turbine performance by assuming the second diffusion loss coefficient to be 0, i.e., assuming no actual turbine diffuser.

A diffuser make the passage smaller and higher velocity. This will potentially increase the losses of the upstream components, e.g., the turbines. Japikse and Baines [74] recommended a value between 0.7 and 0.9 for common diffuser efficiency.

For the multiple horizontal axis turbine configuration, for a diffuser area ratio smaller than 1.3, the area change is assumed to take place before the HTVTS. For a higher diffuser area ratio, the area change before the HTVTS is set to 1.3 and the remaining area change is assumed to take place for the actual diffuser in the SC. Variation of PCU total-to-total efficiency with diffuser area ratio for multiple horizontal axis turbine configuration was shown in Fig. 18 [36]. In this figure, with an increase in diffuser area ratio, the PCU total-to-total efficiency deteriorates significantly, and dropped by 15.3% at the diffuser area ratio of 2. Furthermore, the efficiency increases only slightly by reducing the diffuser area ratio to get a nozzle after the turbine. As shown in Fig. 18, the efficiency increases only by 1.5% with a reduction in diffuser area ratio from 1 to 0.5.

3.3.2.4. Mixing losses. For any multiple turbine configuration, additional losses will be generated where the outflows of various turbines merge. Since more applicable data was lacking, Fluri and von Backström [36] regarded the outflow merging of the various turbines as stream merging in a converging wye when estimating the mixing losses in the geometry of the SC PCU. According to loss coefficients for stream merging in a converging wye reported by Idelchik [75], Fluri and von Backström [36] used a loss coefficient of 0.1 by assuming a wye with converging angle being equal to 15° and equal volume flow through the two branches.

3.3.2.5. HTVTS losses. Without doubt, the HTVTS from the collector outlet to the SC inlet will induce pressure losses. In order to reduce the pressure losses and improve the thermodynamic performance, studies are needed on the transition section.

Kröger and Buys [59] estimated the loss coefficient to be 0.25 for HTVTS of a full-scale plant. This estimated value agrees with the loss coefficient of bell mouth entrance where the curvature radius of the bell mouth profile is equal to about 5% of the diameter for the pipe. von Backström et al. [43] estimated the HTVTS loss coefficient to be 0.161 for a SVSTa based on the measurements of an experimental model. Pretorius [24] compared the annual power outputs obtained by calculating with two estimated values of 0.25 and 0.14 for the loss coefficient of HTVTS. The results showed that the annual power output obtained by calculating with higher loss coefficient at 0.25 was reduced by only 0.4%. Pretorius and Kröger [56] found the annual power output to be reduced by 0.55% for the same comparison for a different configuration plant.

Gannon and von Backström [44] presented velocity profiles just below the turbine. Results showed that the swirl velocity component was remarkably uniform and did not resemble a free vortex. However, they did not present a relationship between IGV angle and the turbine inlet swirl angle.

Kirstein and von Backström [76] studied the flow through the HTVTS of the SCPP with SVSTa designed by Gannon [33] based on the measurement in a scaled model and the simulation with the commercial CFD software CFX to determine the pressure loss coefficient and mean exit swirl angle of the flow passage through the HTVTS of a full-scale SCPP. Table 3 presented the average exit turning angles of the flow passage θ and the total pressure loss coefficients C_L for the four full-scale geometry configurations with different IGV stagger angles ϕ at 22.5° and 31.5° and ratios of collector roof height to SC diameter H_{roof}/D_{ch} at 0.289 and 0.356 by calculating with CFX software which was validated by the measurements (Table 4). For the geometry of configuration A HTVTS, the loss coefficient was equal to 0.056 at full-scale Reynolds numbers [76]. The values were smaller than the previous estimates [24,43,56], which did not consider the Reynolds number scale effect. Based on the simulated results with CFD technology, Kirstein and von Backström [76] also presented empirical expressions of θ and C_L as the functions of ϕ and H_{roof}/D_{ch} for the full-scale geometry

$$\theta = \arctan\left(0.238\frac{\tan\phi}{H_{roof}/D_{ch}}\right) \tag{21}$$

$$C_L = 0.0292 + 0.00114\left(\frac{\sec\phi}{H_{roof}/D_{ch}}\right)^2 + 0.19\tan^2\theta \tag{22}$$

Table 3
Performance of full-scale geometry for four configurations [76].

Configuration	Total pressure loss coefficient	Average exit turning angle (°)
A	0.0558	15.5
B	0.0771	22.9
C	0.0676	18.9
D	0.106	26.7

Table 4
Experimental rig configuration parameters [76].

Configuration	IGV stagger angle (°)	Ratio of collector roof height to SC diameter
A	22.5	0.356
B	31.5	0.356
C	22.5	0.289
D	31.5	0.289

3.3.2.6. Other aerodynamic losses. Compared to the losses due to flow obstructions and components in the PCU, the friction losses in the short straight runs are insignificant and neglected by all the SCPP researchers (e.g., von Backström et al. [43], and Fluri and von Backström [36]). The losses induced by the various struts are neglected by shaping them in streamlined manner to keep the losses low. Windage losses are also neglected [36].

3.3.2.7. Drive train losses. A comprehensive study on the drive train losses of SC turbine has not been reported till now. Fluri and von Backström [36] estimated the drive train losses of SC turbine according to those of wind turbine [77,78]. By taking into consideration industry and market trends, e.g., the steady decline of cost of magnets and power electronics, a configuration with a direct drive permanent magnet generator (DDPM) had a higher potential for further cost reduction than a configuration with a single stage gearbox and a single permanent magnet generator. Bywaters et al. [78] presented the efficiencies of between 90.1% and 92.4% for loads above 25% for a DDPM of 1.5-MW wind turbines only dropping off at very low loads (e.g., 80.8% efficiency at 6% load). Fluri and von Backström [36] used a constant drive train efficiency of 91%, which is assumed for DDPM configurations [78]. For the multiple horizontal axis turbine configuration, drive trains similar to the ones of a large single wind turbine can be used.

3.3.2.8. Total PCU losses. Efficiencies of various PCU components for a reference SCPP under peak power conditions having a collector 7000 m in diameter and SC 1500 high and 160 m in inner diameter by assuming the turbine area is equal to the SC area (i.e., without diffuser) are estimated by Fluri and von Backström [36,79] (Fig. 19). In this figure, the intake, the mixing, and the HTVTS have a very small impact on the overall losses, while the exit losses are significant, with its efficiency reaching at 81.7% [79]. The overall efficiency disregarding the exit losses was 80.1%, which confirmed the assumption of the total-to-total efficiency of the PCU at 80% made by many other researchers (e.g., Pretorius and Kröger [51]). The overall efficiency including the exit losses reached at 65.4%.

3.4. Outflow from SC into atmosphere

The temperature and moisture contents for the SC outflow plume with upward velocity of tens of meters per second are higher than those of the atmosphere at high heights. This will influence the normal distribution of performance (e.g., temperature, velocity, density, humidity) of the atmosphere because the flow and heat transfer of the plume in atmosphere will be produced.

In 2008, Zhou et al. [80] simply analyzed the feasibility of a special climate formed around a commercial SCPP using the Bosanguet I equations [81] which are usually used to calculate rising height of hot flue gases from high industrial SCs (towers) resulting from the combination of initial upward momentum and buoyancy produced by temperature difference in air pollution control engineering. In addition, a great amount of tiny granules in the plume originating from the ground can be used as effective condensation nuclei of moisture. Therefore, super-high power generating SC can increase the chance of rainfall (Fig. 20), even for low-humidity air in the desert region. In 2009, VanReken and Nenes's simulation of the plumes of large-scale SCPP using a cloud parcel model showed cloud would probably form within or downwind of the SC, with precipitation formation possible in some cases [82]. Later, Zhou et al. [83] developed a compressible flow model to simulate the plume from a high power generating SC in an atmospheric cross flow. As expected, the plume induces large fluctuation of the profiles of temperature, velocity, density, relative humidity of atmospheric air. Especially, relative humidity of the plume was greatly increased. A condensation would occur, and a cloud system and precipitation (e.g., rainfall, snow and hail) would be possibly formed around the plume when vapor contained in the plume is supersaturated. It is found that with an increase in SC height or relative humidity of atmosphere, or a reduction in wind velocity, relative humidity is increased, and thus the precipitation probability and the potential precipitation areas. Furthermore, the latent heat released from the condensation of supersaturated vapor can aid the plume to keep on rising. This new special climate can support the agriculture, possibly promote restoration of a part of desert lands, and even create fertile soil and modify the local ecology around the large-scale SCPP [84].

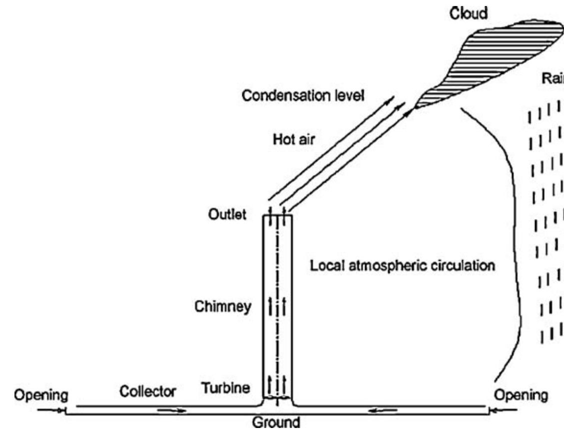


Fig. 20. Schematic diagram of special climate around large-scale SCPP [80].

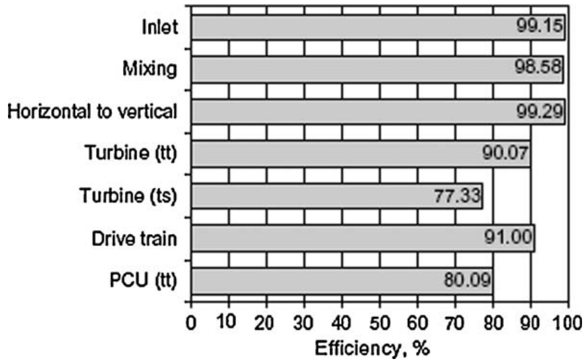


Fig. 19. Efficiencies of various PCU components for a large-scale SCPP without diffuser under peak power conditions [36,79].

4. Study status

4.1. Experiment studies

In the past decades, several experimental models were successively designed, built up, and tested, whose structures differed from each other. The first 50 kW plant prototype built in Manzanares (Fig. 21) in a view to measurement, which had 194.6 m high, 0.00125 m-thickness metallic wall SC guyed and a PVC roof-covered collector 122 m in radius. The main parameters of the Manzanares plant are presented in Table 5. The Manzanares plant has been operating for eight years from 1982 to 1989 [6]. The main operational data, i.e., solar insolation, updraft velocity and power output, were shown on a typical day (June 8, 1987) in Fig. 22 [26]. The power output profile correlates closely with solar insolation profile during day time for this prototype plant without additional storage system, while, there is still an updraft during night time due to thermal storage capacity of natural soil, which can be used to produce power during some hours of the night [19].

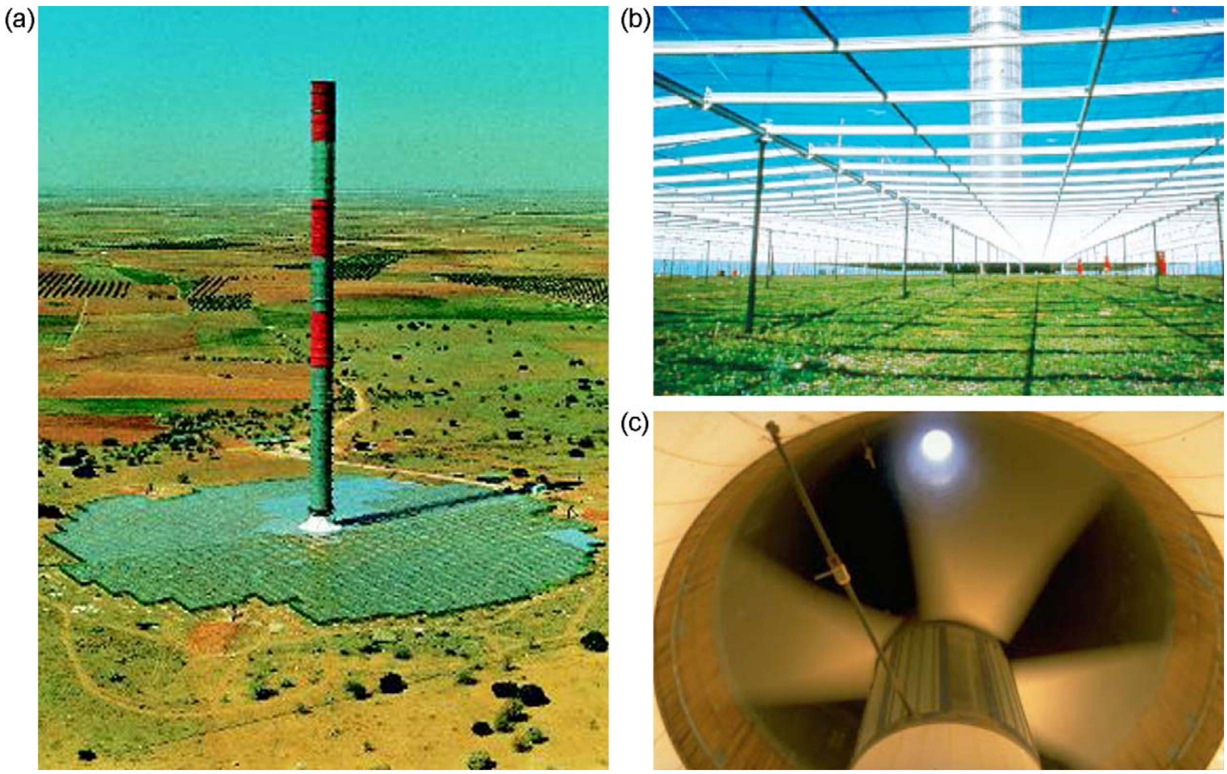


Fig. 21. Pictures of Manzanares plant prototype: (a) whole plant; (b) collector; (c) turbine [5].

In 1983, Krisst [85] built a courtyard SC power setup with 10 W power output. The collector base diameter and SC height were 6 m and 10 m, respectively. In 1985, a micro-scale model with a SC 2 m high and 7 cm in diameter and a 9 m^2 collector was built by Kulunk in Turkey [86].

In 1997, a SC power setup was built by Pasurmarthi and Sherif in Florida, which had a Lexan roof covered collector 9.15 m in diameter and a 7.92 m high SC with its diameter gradually decreasing from 2.44 m at the inlet to 0.61 m at the top (Fig. 23a) [87,88]. An aluminum plate absorber was laid down on the ground under the collector roof (Type I configuration). Two enhancements were tried on the Type I configuration collector to increase the power output. The Type I configuration collector base was extended to form Type II configuration collector 18.3 m in diameter. Black visqueen and clear visqueen with transparency of about 60% were respectively used as the absorber and the roof for the extended parts of Type II configuration collector. An intermediate canvas absorber was introduced between the roof and the aluminum plate absorber inside the Type II configuration collector to improve the conversion efficiency of collector and form Type III configuration collector. The measured air temperature rise and velocity distribution at different locations in the collector were showed in Fig. 24 for the three configuration collectors at an insolation of 650 W/m^2. The Type I configuration collector air temperature rise was about 15 °C, whereas the Type II and Type III collectors were able to raise the temperature by 25 and 28 °C, respectively. These showed the Type I configuration collector was not very effective, and in the Type II and Type III collectors the temperature variation in the extended section was almost the same, whereas in the Lexan roof covered collector section there was a marginal improvement in the Type III collector compared to the Type II collector. In the Type III collector, air flowed on either side of the extended canvas absorber, thus inducing an increase in mass flow rate, and hence power output [87].

A pilot SC setup consisting of an air collector 10 m in diameter and an 8 m high SC was built in Wuhan, China (Fig. 23b) [68,89,90] in 2002 and re-built several times. For up-to-date structure, collector roof and the SC were made of glass 4.8 mm in thickness and PVC, respectively. Temperature difference between the collector outlet and the ambient usually could reach 24.1 °C. An

Table 5
Main structure parameters and technical data of Manzanares plant [6].

Item	Value
SC height (m)	194.6
SC radius (m)	5.08
Mean collector radius (m)	122
Mean roof height (m)	1.85
Number of turbine blades	4
Turbine blade profile	FX W-151-A
Blade tip speed to air transport velocity ratio (m)	10:1
Operation modes	Stand-alone or grid connected mode
Typical collector air temperature rise (K)	$\Delta T = 20$
Nominal power output (kW)	50
Collector covered with plastic membrane (m^2)	40,000
Collector covered with glass (m^2)	6000

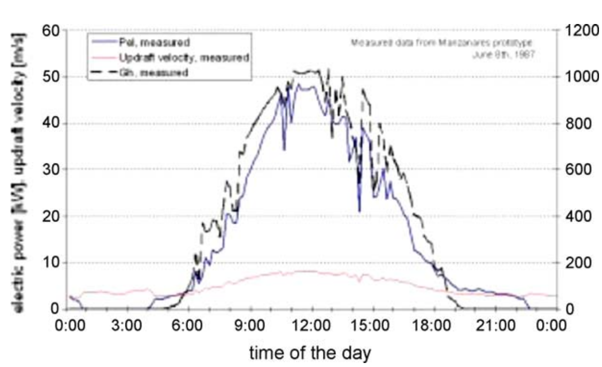


Fig. 22. Measured updraft velocity and power output from Manzanares plant on a typical day (June 8, 1987) [26].

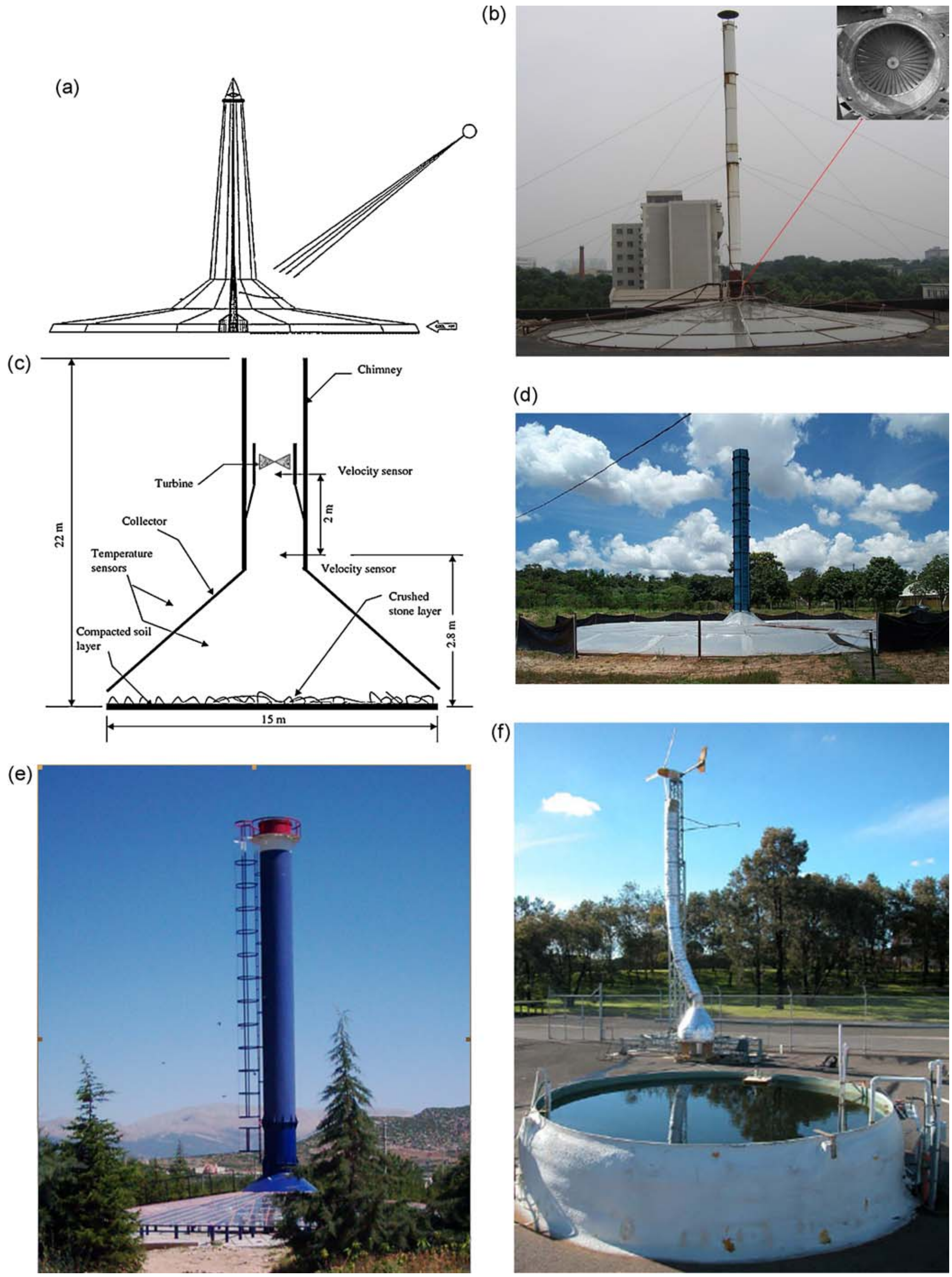


Fig. 23. Pictures or schematic diagrams of other testing models: (a) Sherif et al.'s [87,88]; (b) Zhou et al.'s [68,89,90]; (c) Botswana's [91]; (d) Ferreira et al.'s [92–94]; (e) Koyun et al. [95]; (f) Golder's [96,97].

interesting phenomenon was found that air temperature inversion appeared in the latter SC after sunrise both on a cool day and on a warm day. The air temperature inversion was formed by the increasing process of insolation from the minimum and cleared up some time later when the absorber bed was heated to an high enough temperature to let airflow break through the temperature inversion layer and normally flow out from the SC outlet (Fig. 25).

Based on the need for plans for long-term energy strategies, Botswana's Ministry of Science and Technology designed and built a pilot SC power setup for research (Fig. 23c) [91]. SC was manufactured from glass reinforced polyester material, which had an inner diameter of 2 m and a height of 22 m. The collector roof was made of a 5 mm thick clear glass supported by a steel framework. The collection area reached at approximately 160 m^2. The absorber under the roof was made of two layers of compacted soil approximately 10 mm thick and a layer of crushed stones. The layer of crushed stones was spread on the top surface of the compacted soil layer. This SC power setup ran from October 7 to November 22, 2005. The operating data as shown in Fig. 26 gave insolation, temperature difference and velocity under different conditions: (a) for the selected 5 clear days of October with turbine installed; (b) for the selected 6 clear days between 19 and 30 October with turbine removed; and (c) for 6 days between 14 and 21 November with turbine and diffuser removed. During the time period between approximately 6:00 and 8:00 h, with an increase in insolation from approximately 100 to 500 W/m^2, airflow velocity gradually increased to a high value and then remains nearly constant until approximately 14:00 h, despite the increase in

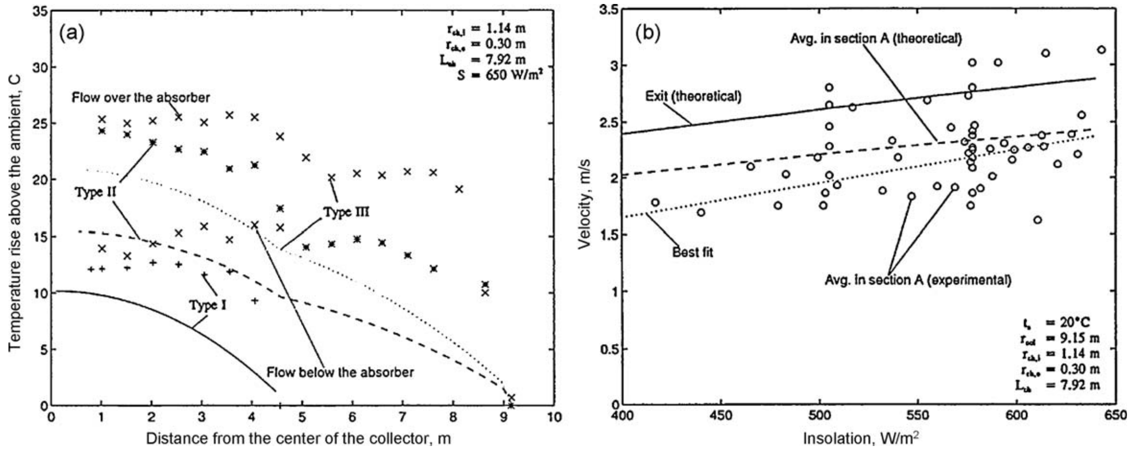


Fig. 24. Measurement from Sherif et al.'s testing model [87]: (a) temperature profiles in three configuration collectors; (b) velocity in Type III configuration collector versus insolation.

insolation to a maximum peak of 950 W/m^2 approximately at 12:00 h. Approximately 47% of incoming solar energy is absorbed and stored by the ground and later released when the local temperature decreases. The temperature difference ranged from about 2 °C at 6:00 a.m. to 7.5 °C at noon, and air velocity ranged from 1 to 2.5 m/s with the diffuser installed and from 2 to 4 m/s with the diffuser removed [91].

A SC power setup was built with a SC 11 m high and 1 m in diameter on the campus of Universidade Federal de Minas Gerais, in Belo Horizonte, Brazil (Fig. 23d) [92–94]. The SC structure was manufactured in five wood modules 2.2 m high each, which was covered internally and externally with glass fiber. The solar collector having a 25 m diameter and a 0.5 m height was built using a plastic film supported by a steel tubular structure.

A pilot SC power setup was also built up on the campus of Suleyman Demirel University, in Isparta, Turkey, which had 15 high SC 1.2 in diameter and a glass covered collector 16 m in diameter [95].

A small prototype demonstrating the combination of an experimental solar pond of approximately 4.2 m diameter and 1.85 m dept with a SC 8 m high and 0.35 m in diameter was constructed by Golder in the campus of RMIT University, in Bundoora, Australia in 2002 (Fig. 23f) [96,97]. The water to air heat exchanger was equipped at the SC base. The SC was manufactured from flexible circular ducting which was insulated with 60 mm thick fiberglass, and supported by the structure of a small experimental aero generator within a few meters of the solar pond. Hot brine was extracted from the solar pond at a rate of 1.21 liter per minute through a diffuser placed at approximately 0.5 m above the bottom of the pond and was pumped through the heat exchanger. After delivering its heat to the air which passed through the heat exchanger and SC, the cooler brine was returned to the bottom of the pond through a second diffuser. The measurements showed that for a solar pond temperature of 45 °C, the temperatures of the brine entering and exiting the heat exchanger could reach 37 °C and 25 °C, and the entering air through the heat exchanger was raised from the outside ambient temperature of 17 °C to an exit temperature of about 28 °C. An air flow velocity in the SC was measured at 1 m/s.

4.2. Theoretical studies

After Schlaich's pioneer work on the SC concept to harness solar energy, many researchers, e.g., Haaf et al. [15], Lautenschlaqer et al. [67], Louis [98], Mullett [63], Padki and Sherif [99–102], Yan et al. [30], Lodhi [64], Bernardes et al. [29], Schlaich et al. [26,103,104], von Backström and coworkers [32–34,42–45,71,105], Bernardes et al. [55], Dai et al. [106], Zhou et al. [68,107–111], Ninic and coworkers [112,113], Nizetic and Klarin [114], Pastohr et al. [65], Onyango and Ochieng [66], Ming et al. [115–118], Koonsrisuk and Chitsomboon [119–123], Chergui and coworkers [124–127], and Petela [128], provided theoretical modeling investigations for large-scale SCPP. Pretorius [24,51] performed the comprehensive studies on air flow and heat transfer in large-scale SCPP.

The typical daily power output profile during summer and winter for a reference large-scale SCPP [24] was shown in Fig. 27a, which had a collector 5000 m in diameter and a SC 1000 m high with 210 m inner diameter. Two typical effective methods of controlling and enhancing power output from SCPP include

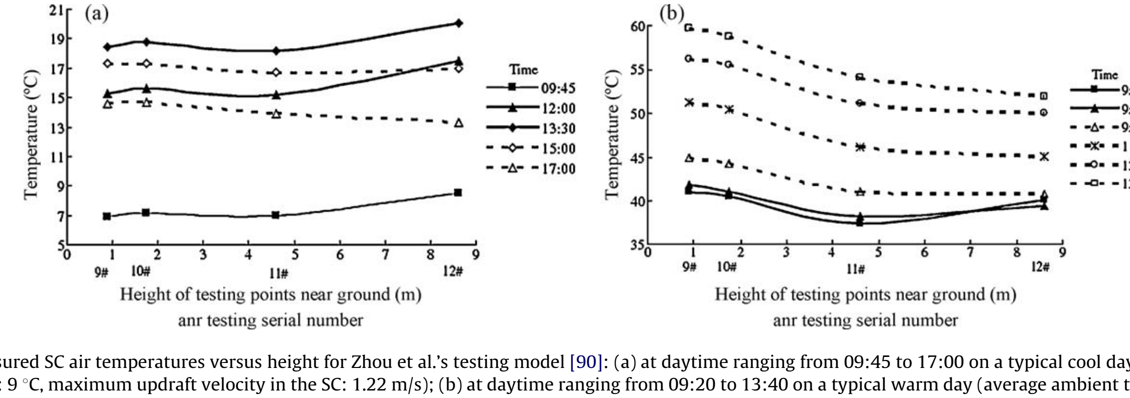


Fig. 25. Measured SC air temperatures versus height for Zhou et al.'s testing model [90]: (a) at daytime ranging from 09:45 to 17:00 on a typical cool day (average ambient temperature: 9 °C, maximum updraft velocity in the SC: 1.22 m/s); (b) at daytime ranging from 09:20 to 13:40 on a typical warm day (average ambient temperature: 28 °C, maximum updraft velocity in the SC: 2.81 m/s).

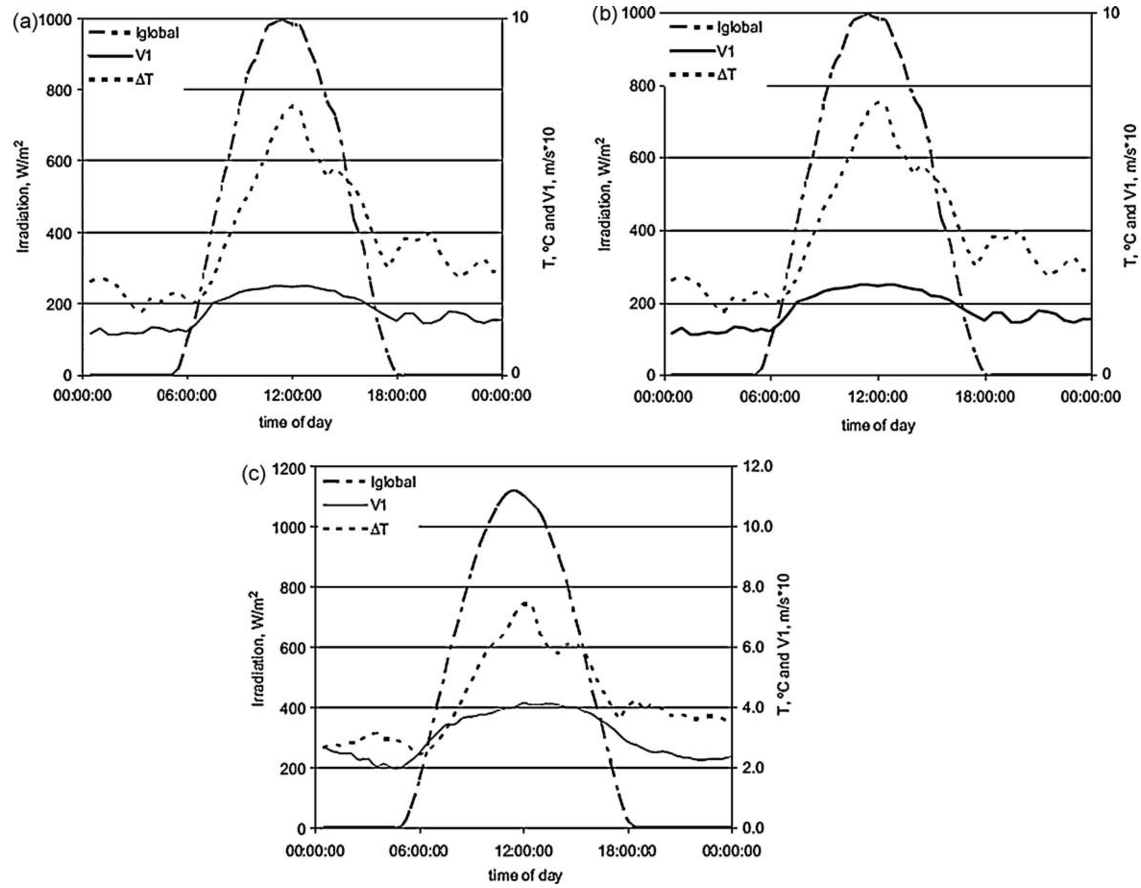


Fig. 26. Average of measured insolation, temperature difference and velocity [91]: (a) for selected 5 clear days of October (with turbine installed); (b) for selected 6 clear days between 19 and 30 October (with turbine removed); (c) for 6 days between 14 and 21 November (with turbine and diffuser removed).

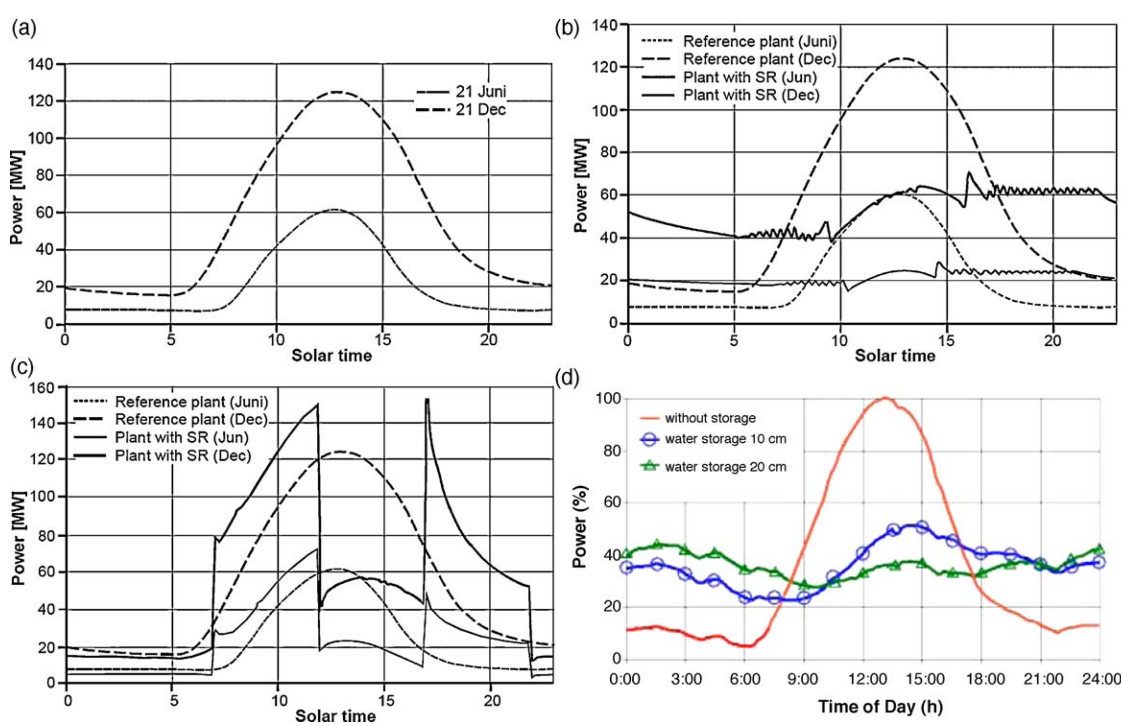


Fig. 27. Daily power output profiles for large-scale SCPP both without and with effective performance-controlling system: (a) without effective performance-controlling system [24]; (b) with intermediate secondary roof as base load [24]; (c) with intermediate secondary roof as peak load [24]; (d) with additional closed water-filled thermal storage system [26].

introducing intermediate secondary roof under the first collector roof and additional closed water-filled thermal storage system on the ground as referred to in Section 2.1. Daily power output profiles for the reference SCPP with intermediate secondary roof as base load and peak load were respectively shown in Fig. 27b and c. The results showed that intermediate secondary roof gave a much more uniform daily output profile compared to a plant with single roof. The incorporation of additional closed water-filled system [25,26] was also proved to be a good mechanism for a power output controlling and enhancing, which gave a much more uniform daily output profile compared to a plant without such closed water-filled system (Fig. 27d).

5. Economics

5.1. Economics for power generation

In order to assess the economics and competitiveness of SCPP, economic analyses were performed by several researchers, e.g., Schlaich [6], Schlaich et al. [104] and Bernardes [54]. Schlaich [6] estimated the costs for all plant components for various plant sizes. He also evaluated the levelised electricity cost (LEC) and performed the sensitivity analysis of LEC to the interest rate and the length of the depreciation period. Schlaich et al. [104] presented the component costs and the LEC for various plants for fixed economic parameters. Bernardes [54] also estimated the component costs and LEC of various-size SCPP, and performed the sensitivity analysis of LEC to the economic parameters. In addition to that, he derived a parametric cost model for the main plant components, i.e., collector, SC and PCU.

Fluri et al. [129] presented a more detailed cost model, including a first detailed cost model for the PCU, where the impact of carbon credits on LEC was also considered, and compared the results to Schlaich et al. [104] and Bernardes [54]. For the purpose of comparison, two reference SCPPs with similar sizes as the 100 MW plants respectively proposed by Schlaich et al. [104] and Bernardes et al. [54] were selected. In the detailed cost model, the SC cost includes the material cost, construction cost, hoisting cost, and transport cost, the collector cost includes the material cost, construction cost, and transport cost, and the PCU cost includes the cost of balance of station, generators, turbines, ducts, power electronics, central structure, controls, and supports. Costs of the two reference SCPP components calculated using the model and their comparison to the values in literatures [54,104] can be presented in Tables 6–8. Fluri et al. [129] estimated the power output of the reference SCPPs using Pretorius's thermodynamic model [24]. The simulation results showed a lower peak power output of 66 MW for Schlaich et al.'s reference plant, and 62 MW for Bernardes's reference plant, instead of 100 MW. LEC for the Schlaich et al.'s 100 MW plant therefore reached at a higher value of €0.270/kWh than Schlaich et al.'s at €0.1/kWh with the same

Table 6
Comparisons of costs of SCPP components calculated by Fluri and von Backström [129] to Schlaich et al.'s [104] and Bernardes's calculations [54].

Component cost	Schlaich et al.		Bernardes	
	Fluri and von Backström's cost	Rel. to Schlaich et al.	Fluri and von Backström's cost	Rel. to Bernardes
SC	M€145	93%	M€111	172%
Collector	M€497	379%	M€656	345%
PCU	M€27	36%	M€25	33%
Total investment	M€668	166%	M€792	225%
Specific investment	€10,025/kW	249%	€12,766/kW	362%

Table 7
Comparisons of LEC calculated by Fluri and von Backström [129] to Schlaich et al.'s calculations [104].

	Schlaich et al.	Fluri and von Backström
Annual power output (GWh)	320.0	190.4
Capital cost (M€)	402.0	668.4
Cumulative PV of OM (M€)	34.9	38.9
LEC (€/kWh)	0.1	0.270
LEC considering carbon credits (€/kWh)		0.232

Table 8
Comparisons of LEC calculated by Fluri and von Backström [129] to Bernardes's calculations [54].

	Bernardes	Fluri and von Backström
Annual power output (GWh)	281.0	181.3
Capital cost (before construction) (M€)	325.4	791.5
Capital cost (after construction) (M€)	379.5	923.2
Cumulative PV of O&M (M€)	15.59	15.59
LEC (€/kWh)	0.125	0.430

economic parameters (i.e., interest rate = 6%, inflation rate = 3.5%, and depreciation period = 30 years). LEC for the Bernardes's 100 MW plant at €0.43/kWh is far larger than the value at €0.125/kWh re-calculated using Bernardes's model with the same economic parameters (i.e., interest rate = 8%, inflation rate = 3.25%, depreciation period = 30 years, and construction period = 2 years). (Fluri et al. [129] thought a very low LEC at €0.037/kWh actually quoted by Bernardes [54] was caused by an error in calculation). During operating period, the SCPP avoids the CO_2 emissions from coal-fired power plant, which typically emits 0.95 kg of CO_2 per kWh power output [130]. Large amount of carbon credits was therefore obtained for SCPP. The fact that SCPP construction will need to consume fossil fuels is neglected because the coal-fired power plant construction also needs to consume fossil fuels, and long service life of reinforced concrete SC corresponds to the total of service life of two to three coal-fired power plant. When the potential impact of carbon credits on LEC is included in this model, the LEC decreases a little, for example, the LEC of Schlaich et al.'s 100 MW plant decreases to €0.232/kWh. In usual, the reinforced concrete SC could use for more than 80 years, which would lead to further reduction in SCPP LEC.

5.2. Additional revenues

A great concern with all solar technologies is extensive use of lands because of low energy concentration of sunlight. The investment of large-scale SCPP is large, and the solar collector is the main cost factor of SCPP as shown in Section 5.1. Additional revenue sources linked to the collector would be highly welcomed. The best additional use of a solar collector would be for growing vegetables or fruits as a greenhouse for possible additional revenues. The ground under the collector roof requires to be irrigated with fresh water. However, fresh water could be scarce in the potential construction sites of SCPPs, which are often selected in deserts, where land is cheap and sunlight is abundant. In order to grow vegetables or fruit, some lands are selected for the locations of SCPP, which aren't yet deserts but are threatened to become a desert if the climate change goes on, or which has recently become a desert. With pleasure, a wet cultivated ground is often darker than a dry flat one, so that this albedo effect generates a synergy among agricultural and power productions. However, solar heating of an irrigated ground would generate much evaporation, i.e., convert parts of solar heat to latent heat, thus reducing power output largely.

According to this principle, since 1998, South African researchers [131] have designed and performed experimental and theoretical study on a mixed project of a SCPP and a large, possibly profitable greenhouse for additional agricultural use. In the greenhouse, some black 'shadowing nets' were used, whose purpose might be multiple [132]. During day time, these black shadowing nets will absorb solar radiation, and provide the main source of sensible heat to the moving air, which will be hotter than the agricultural greenhouse air. So, quite no convection will drive both airs to switch their places. During night time, the ground is hotter than the black shadowing nets. This will drive air convection from the ground to the black shadowing nets. Black shadowing nets can be the thermal contact point between cold collector operating air and the agricultural greenhouse mild warm air. When evaporated water coming from the ground is recondensed at the colder lower surface, the heat exchange would produce some dew, which will fall back to the humus. The 'shadowing nets' prevent steam from escaping into the SC, without wasting the fresh water and the latent heat.

Such a structure with 'shadowing nets' will give the whole system a very dark albedo. Of course, shadowing a greenhouse could slow down the photosynthesis, but, in very sunny regions, temperature and hygrometry regulations are an asset, especially if these shadowing nets can be adapted to the light conditions all the day.

In addition to use for heating collector operating air, at the same time, additional use of the outer 2/3 of solar collector area as greenhouse can increase production of a highly productive agricultural area from 100% to at least 270%, adding a virtual 170% to the existing land. Furthermore, vegetation in the collector also could increase heat and power production. These conclusions are mainly drawn based on Prof. Kröger's experimental and theoretical studies in 2000 [131].

6. Other types of SC power technology

6.1. Floating SC power technology

The conventional SC used for power generation is constructed by reinforced concrete. Although having a long service life, the reinforced concrete SC, whose height is required to be as high as possible in order to improve the efficiency of SCPP, has some disadvantages. The disadvantages include high construction cost and limited height because of the technological constraints and restrictions on the construction materials. There are also external limitations such as possible earthquakes, which can easily destroy super high SCs. Based on these facts, Papageorgiou [133,134] proposed a floating solar chimney (FSC) concept instead of reinforced concrete SC to be used for SCPP.

FSC consists of three parts: main body, heavy base and folding lower part, as shown in Fig. 28a and b. The main body is composed of buoyant gases-filled cylindrical balloon rings tied up to each other with the help of supporting rings. The main body is fastened to the seat of the heavy base and the folding lower part is fastened to the lower part of the heavy base, which can withstand the exterior winds by letting the air enter and come out freely from its rings so that FSC can receive any suitable declination exposed to wind.

Papageorgiou [135–140] designed the FSC structure, and performed some work on FSC power plant, including investigation of external wind effect and optimum design of SCPP. Zhou et al. [141] performed economic analysis of FSC power plant using an economic model. Later, they [142] proposed a novel solar thermal power plant with FSC stiffened onto a mountain-side, segment by segment (Fig. 29) and estimated the potential of the power generation of the system in China's deserts.

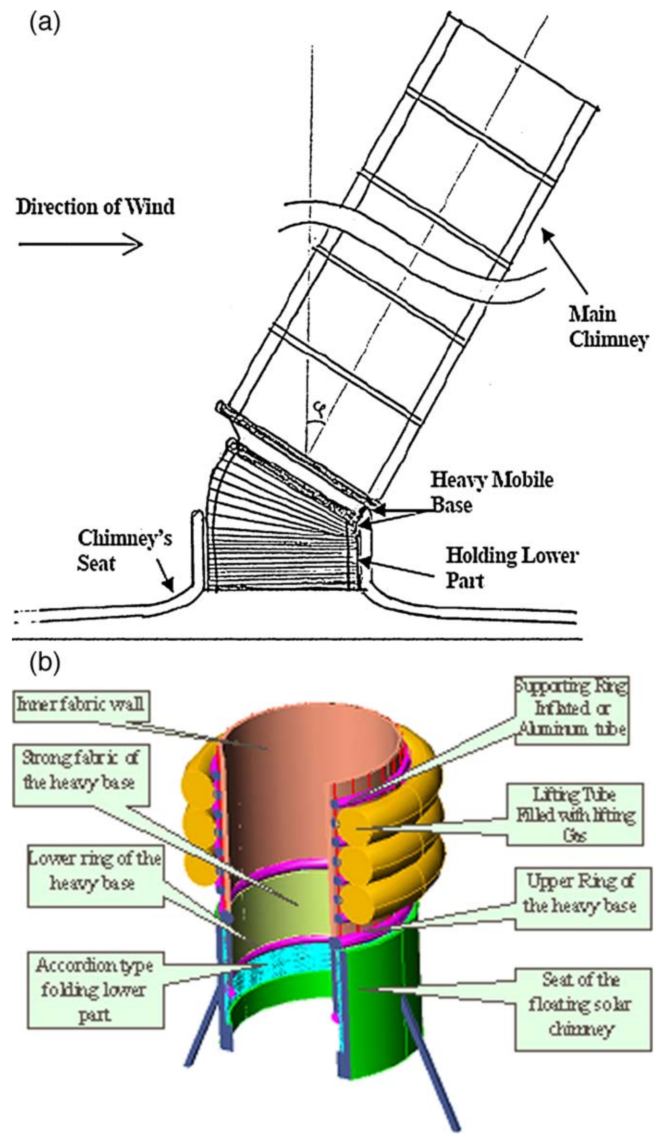


Fig. 28. (a) Schematic diagram of FSC exposed to wind [133]; (b) detailed schematic diagram of FSC [134].

6.2. SC power technology with sloped collector

The novel concept consisting of a sloped collector and a short SC was proposed by Bilgen and Rheault [143], as shown in Fig. 30.

Collector has a triangular surface area with a SC at its apex. The sides are closed, and air enters from the lower side and rises as heated by the ground to the apex where a short SC is installed vertically. Practically, this sloped collector also plays a 'SC' effect due to the climbing of slope absorber under the collector roof.

Bilgen and Rheault [143] developed a mathematical model for this new type of SC power system. By assuming that air density linearly changes from the collector inlet to outlet, the collector inward air density can be expressed as

$$\rho = \rho_\infty + \frac{\rho_2 - \rho_\infty}{H_{coll}} h \quad (23)$$

Substituting Eq. (23) into Eq. (11), one obtains

$$\Delta p_{coll} = \frac{\rho_\infty - \rho_2}{2} g H_{coll} \quad (24)$$

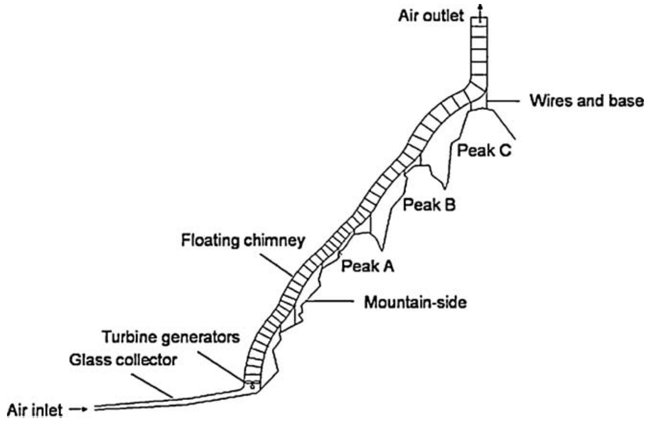


Fig. 29. Novel solar thermal power plant with a floating chimney stiffened on a mountainside, segment by segment [142].

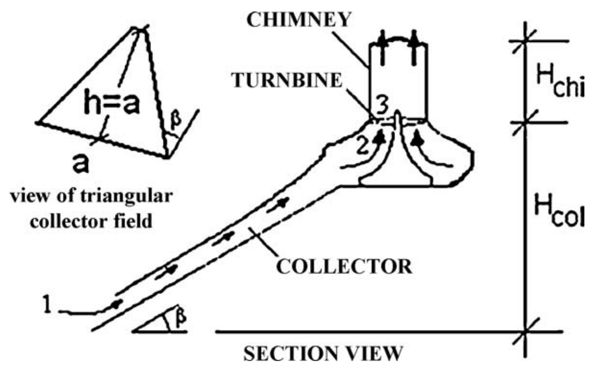


Fig. 30. Schematic diagram of SCPP with sloped collector [143].

The total pressure potential is further expressed as

$$\Delta p = (\rho_{\infty} - \rho_2) g \left(H_{ch} + \frac{H_{coll}}{2} \right) \quad (25)$$

where $H_{coll} = \sqrt{2 \cdot A_{coll}} \cdot \sin\beta_{opt}$ with β_{opt} being the optimal slope of collector.

It was shown from Eq. (25) that the effective 'SC height' was equal to $(H_{ch} + H_{coll}/2)$.

Bilgen and Rheault [143] performed parametric analysis to optimize the collector slope to maximize insolation received by solar collector for three locations, Ottawa, Winnipeg, and Edmonton at high altitude, respectively, whose latitudes changed from 45.5°N to 49.9°N to 53.6°N. The results showed that the optimum slope of collector should be 5–7° smaller than the altitude. A thermo-dynamic simulation study was conducted to determine the design parameters and operational data for 5 MW SCPPs (Table 9). The thermal performance of the SC power technology with sloped collector is slightly higher than that with the conventional horizontal collector.

Wei et al. [144] also analyzed the slope's effect for receiving insolation and investigated on the optimal slope of collector in SCPP.

In the mid and high latitudes, the conventional horizontal solar collector can not receive the sunshine perpendicularly. The collector on an appropriate slope will reduce the incidence angle, thus increasing insolation received by the collector. The SC power technology with sloped collector can be effective technology applied at mid and high latitudes.

6.3. SC power technology with mountain hollow

The novel concept consisting of a design for constructing a giant solar collector surrounding a hollow space excavated in a mountain in a steady-geology region (Fig. 31) was proposed by Zhou et al. [145]. The giant hollow space in the mountain is excavated as an updraft 'SC'.

Fig. 31a and b, respectively, gave a top view and a vertical view of a prototype with the novel concept for producing energy integrating a solar collector with a man made mountain hollow. The hollow space can be used as an economical and safe updraft 'SC'.

Table 9
Designed parameters for 5 MW SCPPs with sloped collector and their comparisons to Schlaich's calculations [143].

	Ottawa	Winnipeg	Edmonton	Schlaich [5]
Collector diameter (m)	–	–	–	1110
Collector area (m^2)	950,000	950,000	950,000	950,000
SC height (m)	123	60	35	547
Collector height (m)	848	975	1024	–
SC diameter (m)	54	54	54	54
Collector air temperature rise (K)	25.9	25.9	25.9	25.9
Updraft velocity (m/s)	9.1	9.1	9.1	9.1
Total pressure head (Pa)	518.3	518.3	518.3	383.3
Average efficiency				
Collector (%)	56	56	56	56.24
SC (%)	1.82	1.82	1.82	1.45
Turbine (%)	77	77	77	77
Whole system (%)	0.79	0.79	0.79	0.63

6.4. SC power technology for harvesting atmospheric water

Kashiwa et al. [146,147] proposed a novel concept 'Solar cyclone' for harnessing solar energy, and for extracting fresh water from atmosphere on the earth's surface (Fig. 32). Fig. 32 shows one configuration for the Solar cyclone and illustrates the principle of operation of the expansion cyclone separator [146]. Compared with conventional SCPP, an expansion cyclone separator for condensing and removing atmospheric water is placed behind the turbines at the SC base. Swirl vanes installed in the collector cause the radial warm inflow to rotate. The radial and the swirl components of the velocity of the swirling flow will increase when moving toward the SC base. This is accompanied by a reduction of temperature, pressure and density. The air will drive the turbines to power generators in the center, and then vertically enter into the separator.

The separator, which consists of a strongly rotating vortex, has the shape of a converging–diverging nozzle, where inflow is rotating. The mean temperature of air flow drops well below the dew point in the converging part, where condensation of a fog immediately occurs with the help of some amount of dust always contained in the surface air, intense turbulence causes rapid growth of droplets, centrifugal action moves droplets to the wall in the nozzle throat where a rotating film of water is guided into a collection trap. A small negative pressure, relative to the throat pressure, is maintained by a venturi effect in the collection trap in order to promote flow of the film into the trap.

This Solar cyclone could produce not only electric power but also fresh water. Kashiwa et al. [146] simply analyzed the capacity of products for a single Solar cyclone 500 m high and 42 m in diameter. The results showed that by assuming a separation efficiency of 80% the Solar cyclone can produce annual power output of 3 MW and annual fresh water production of 2×10^6 tonnes in an arid region. This could satisfy the household fresh water needs, and about 75% of the electrical needs, for an urban population of 10,000 residents in an arid region. As expected, fresh water and power production increased exponentially with the SC height ranging from 0 to 1000 m, as shown in Fig. 33.

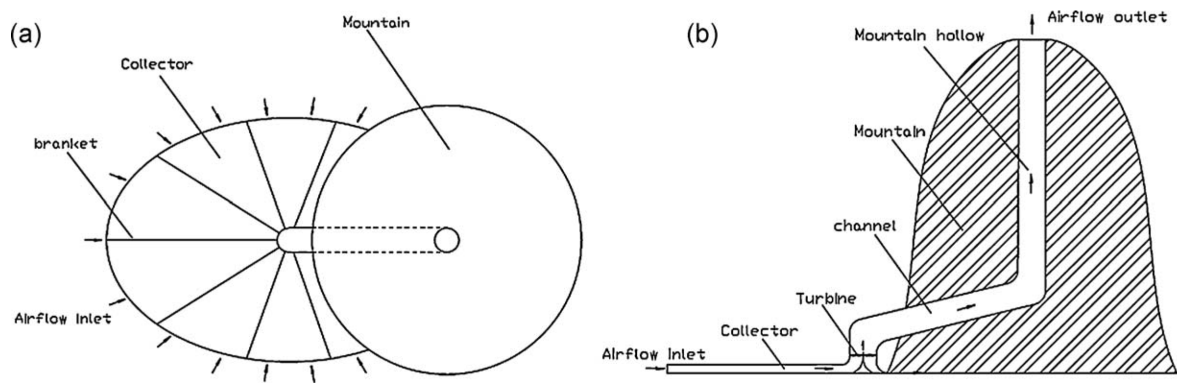


Fig. 31. Schematic diagram of SCPP with mountain hollow SC [145]: (a) top view and (b) vertical view.

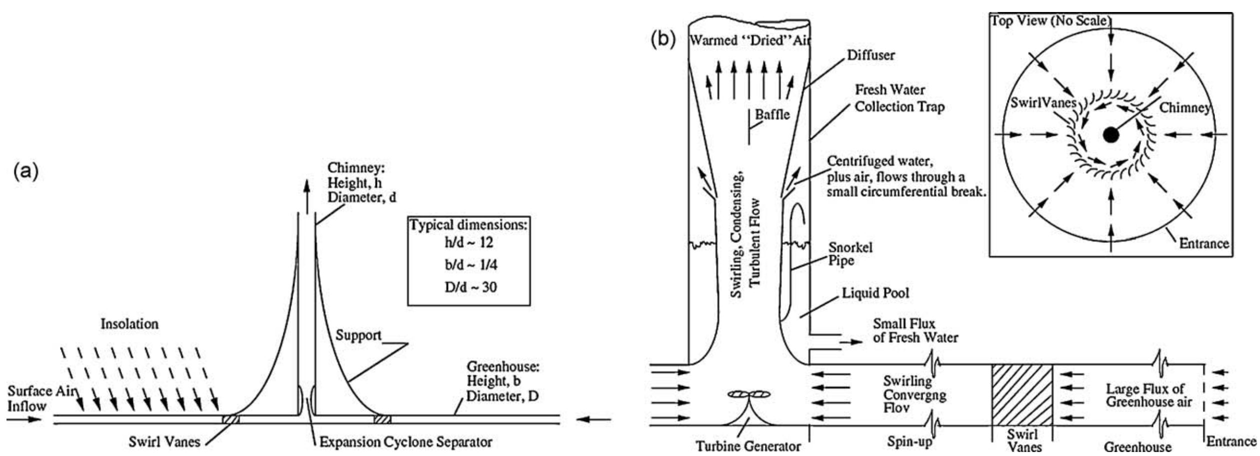


Fig. 32. Schematic diagram of SCPP for harvesting atmospheric water [146]: (a) Solar cyclone, (b) expansion cyclone separator.

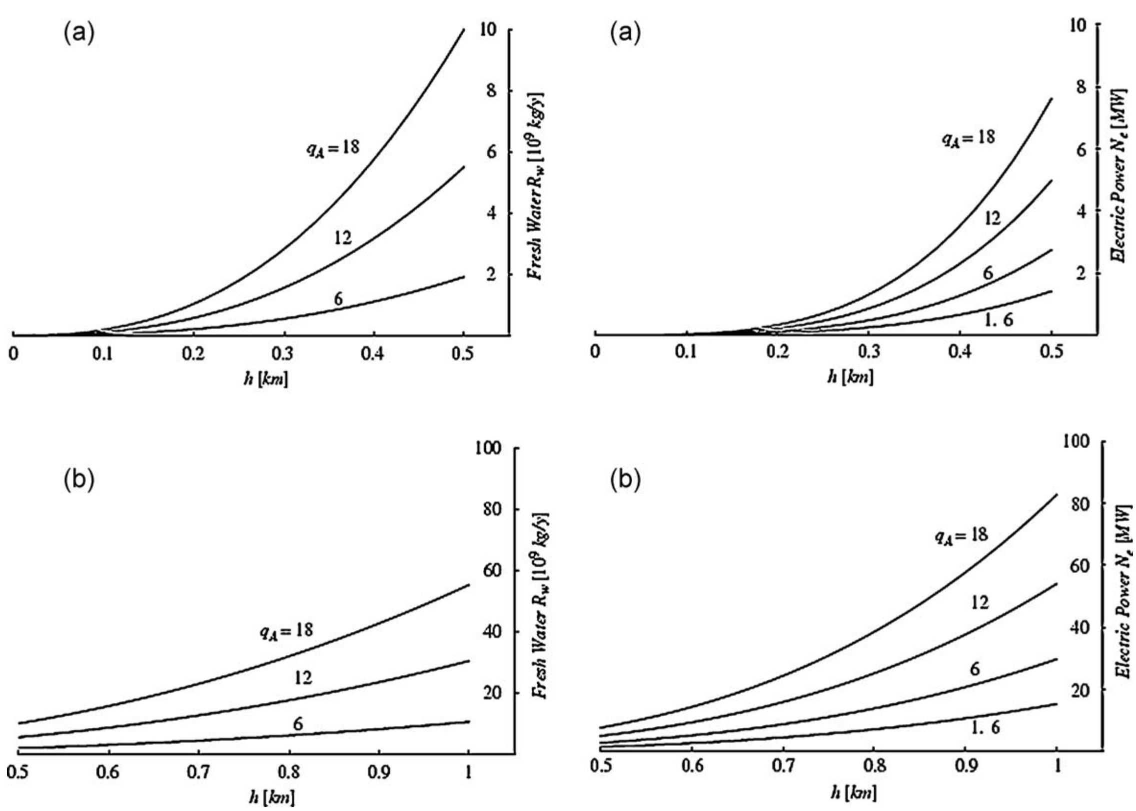


Fig. 33. Fresh water production and electric power versus height [146]: (a) 0 km $\leq h \leq$ 0.5 km; (b) 0.5 km $\leq h \leq$ 1 km.

6.5. Other combined SC power technologies

Günther [12] presented another concept of SC power technology with SC supported by mountain. Zhou et al. [148] also analyzed the potential of application of this technology in China.

Wang et al. [149,150] proposed the combined SC system for both power generation and seawater desalination suitably at a site adjacent to the sea by installing a high-efficiency condenser at the SC inlet or the outlet, respectively. In the combined SC system, seawater pumped from the sea opens to air in the collector where warm and saturated operating air is produced by solar energy. In the system where high-efficiency condenser was placed at the SC inlet, the vapor contained in warm and saturated operating air is condensed and fresh water is produced. The operation principle for the configuration with high-efficiency condenser placed at the SC outlet was more complicated than that for the configuration with high-efficiency condenser placed at the SC inlet. In the former system, the vapor contained in the warm inflow is condensed to water using a high-efficiency condenser, and fresh water holding big gravitational potential energy is used for power generation by driving water turbine generators installed at ground level. The products from the power plant include electric power from air turbine generators and water turbine generators and fresh water, though the electric power from air turbine generators is far less than the same-scale conventional SCPP because much heat is used as latent heat of water evaporation to reduce the buoyancy in the combined SC system [23]. Additionally, the performances of the two systems change at different sites where there are different climate conditions and prices of electricity and fresh water in the market. So, there is a better choice between the system and the conventional SC power system to maximize the revenue of products at a given site. Zhou et al. [151] compared the performance and economics of the conventional SC power system and the combined SC system for power generation and seawater desalination.

7. Discussions and conclusions

SC power technology is a simple solar thermal power technology, which includes three familiar technologies: solar collector, SC, and PCU, e.g., turbine generators. In order to improve the SCPP performance, some other configurations and layouts were proposed for the components. The detailed discussion about the complex losses (namely aerodynamic, mechanical and electrical losses) in the PCU showed that the overall efficiency disregarding the exit losses could reach 80.1%. The experimental and theoretical study status was reviewed. For controlling and enhancing SCPP's power output profile, three measures were proposed to be taken including to introduce an intermediate secondary roof under the first roof and to lay a closed water-filled thermal storage system down on natural soil, and to use solar ponds for thermal storage of SCPP. The theoretical studies on the large-scale SCPP showd the first two measures were good controlling mechanisms, which gave much more uniform daily output profiles than without any controlling mechanism. LEC of SCPP is a little higher than the coal-fired power plant, but will be reduced by considering zero pollutant emissions and additional revenues of the solar collector. With the research and development of new materials, and the escalation of the contradiction between further rapid reduction of fossil fuel reserves and large increase in the energy needs, the SC power technology will possibly play an important role in world development in future, which uses insolation for power generation in vast desert regions.

Acknowledgement

Thanks to data supplied by Dr. Denis Bonnelle. This research has been supported by the National Natural Science Foundation of China under Grant No. 50908094, and the Youth Chenguang Project of Science and Technology of Wuhan City of China under Grant No. 201050231076.

References

[1] Service RF. Is it time to shoot for the sun. Science 2005;309:548–51.
[2] Gullison RE, Frumhoff PC, Canadell JG, Field CB, Nepstad DC, Hayhoe K, et al. Tropical forests and climate policy. Science 2007;316:985–6.
[3] Kerr RA. Global warming is changing the world. Science 2007;316:188–90.
[4] Kerr RA. Climate change: Is battered arctic sea ice down for the count? Science 2007;318:33–4.
[5] Stern N. The economics of climate change: the Stern Review. Cambridge, UK: Cambridge University Press; 2007.
[6] Schlaich J. The solar chimney: electricity from the sun. Stuttgart, Germany: A. Menges; 1995.
[7] Dennis C. Solar energy: radiation nation. Nature 2006;443:23–4.
[8] Woody T. Tower of power. In: The 31 best business ideas in the world. Business 2.0 2006;7:94–102.
[9] Papageorgiou CD. Floating solar chimney: the link towards a solar future. In: Proceedings of the ISES 2005 solar world congress conference; August 2005.
[10] Zhou XP, Yang JK, Xiao B, Hou GX, Shi XY. Special climate around a commercial solar chimney power plant. J Energy Eng Trans ASCE 2008;134:6–14.
[11] Cabanyes I. Las chimeneas solares (Solar chimneys). La ernergia eléctrica. Cited due to Wikipedia; 1903.
[12] Günther H. In hundert Jahren – Die künftige Energieversorgung der Welt (In hundred years – Future energy supply of the world). Kosmos, Franckh'sche Verlagshandlung, Stuttgart; 1931.
[13] Lucier RE. Apparatus for converting solar to electrical energy. US. Patent; 1979.
[14] Pasumarthi N, Sherif SA. Experimental and theoretical performance of a demonstration solar chimney model. Part I: Mathematical model development. Int J Energy Res 1998;22:277–88.
[15] Haaf W, Friedrich K, Mayr G, Schlaich J. Solar chimneys. Part I: Principle and construction of the pilot plant in Manzanares. Int J Solar Energy 1983;2:3–20.
[16] Robert R. Solar prototype development in Span show great promise. MPS Rev 1982;(2):21–3.
[17] Robert R. Hot air starts to rise through Span's solar chimney. Electr Rev 1982;210(15):26–7.
[18] Castillo MA. A new solar chimney design to harness energy from the atmosphere. Spirit of enterprise: the 1984 Rolex Awards; 1984. p. 58–9.
[19] Haaf W. Solar chimneys, part II: preliminary test results from the Manzanares pilot plant. Int J Solar Energy 1984;2:141–61.
[20] EnviroMission Limited Inc. Clean, green renewable energy: technology overview. Available at: http://www.enviromission.com.au/IRM/content/technology_technologyover.html.
[21] Torre solar de 750 metros de altura en Ciudad Real (España). http://www.astroseti.org/vernew.php?codigo=2188.
[22] Cloete R. Solar tower sheds light on little-used technology. Engineering News Online. http://www.engineeringnews.co.za/article.php?a_id=137580. 2008-07-25. Retrieved on 2008-10-17.
[23] Bonnelle D. Solar chimney, water spraying energy tower, and linked renewable energy conversion devices: presentation, criticism and proposals. Doctoral thesis. Lyon 1, France: University Claude Bernard; July 2004. Registration Number: 129-2004.
[24] Pretorius JP. Optimization and control of a large-scale solar chimney power plant. Ph.D. thesis. South Africa: University of Stellenbosch; 2007.
[25] Kreetz H. Theoretische Untersuchungen und Auslegung eines temporaren Wasserspeichers fur das Aufwindkraftwerk. Diplomarbeit. Berlin: Energie und Verfahrenstechnik der TU Berlin; 1997.
[26] Schlaich J, Bergermann R, Schiel W, Weinrebe G. Design of commercial solar updraft tower systems—utilization of solar induced convective flows for power generation. J Solar Energy Eng 2005;127:117–24.
[27] Davey RC. Device for generating electricity from solar power. WO 2008/022372 A1; 28 February 2008.
[28] Fraser J. EnviroMission's Solar tower of power. Available at: http://energy.seekingalpha.com/article/14935, August 3, 2006.
[29] Bernardes MA dos S, Valle RM, Cortez MF. Numerical analysis of natural laminar convection in a radial solar heater. Int J Therm Sci 1999;38:42–50.
[30] Yan MQ, Sherif SA, Kridli GT, Lee SS, Padki MM. Thermo-fluids analysis of solar chimneys. Ind Applic Fluid Mech 1991;ASME FED-2:125–30.
[31] Müller M. Dreidimensionale Simulation der Strömungskontur eines Aufwindkraftwerks (Three dimensional simulation of the flow in a solar chimney power plant). Student research project, Institut für Strömungsmechanik und hydraulische Strömungsmaschinen, Universität Stuttgart; 2002 [in German].
[32] von Backström TW, Gannon AJ. Solar chimney turbine characteristics. Solar Energy 2004;76:235–41.
[33] Gannon AJ. Solar chimney turbine performance. Ph.D. thesis. South Africa: University of Stellenbosch; 2002.
[34] Gannon AJ, von Backström TW. Solar chimney turbine part 1 of 2: design. In: International solar energy conference. 2002. p. 335–41.
[35] Fluri TP. Turbine layout for and optimization of solar chimney power conversion units. Ph.D. thesis. University of Stellenbosch; 2008.
[36] Fluri TP, von Backström TW. Performance analysis of the power conversion unit of a solar chimney power plant. Solar Energy 2008;82:999–1008.

[37] Schwarz G, Knauss H. Strömungstechnische auslegung des aufwindkraftwerks Manzanares (Aerodynamic design of the solar chimney power plant in Manzanares), Techical report, Institut für Aerodynamik, Unversität Stuttgart; 1981 [in German].
[38] Denantes F, Bilgen E. Counter-rotating turbines for solar chimney power plants. Renewable Energy 2006;31:1873–91.
[39] Fluri TP, von Backström TW. Comparison of modelling approaches and layouts for solar chimney turbines. Solar Energy 2007;82:239–46.
[40] Schlaich J. Tension structures for solar electricity generation. Eng Struct 1999;21:658–68.
[41] Harte R, Van Zijl GPAG. Structural stability of concrete wind turbines and solar chimney towers exposed to dynamic wind action. J Wind Eng Ind Aerodyn 2007;95:1079–96.
[42] Gannon AJ, von Backström TW. Solar chimney cycle analysis with system loss and solar collector performance. J Solar Energy Eng 2000;122:133–7.
[43] von Backström TW, Bernhardt A, Gannon AJ. Pressure drop in solar power plant chimneys. J Solar Energy Eng 2003;125:165–9.
[44] Gannon AJ, von Backström TW. Solar chimney turbine performance. J Solar Energy Eng 2003;125:101–6.
[45] von Backström TW, Gannon AJ. Compressible flow through solar power plant chimneys. J Solar Energy Eng 2000;122:138–45.
[46] Sawka M. Solar chimney-untersuchungen zur strukturintegrität des stahlbetonturms. Bergische Universität Wuppertal; 2004.
[47] Busch D, Harte R, Krätzig WB, Montag U. New natural draft cooling tower of 200 m of height. Eng Struct 2002;24:1509–21.
[48] Graffmann M, Harte R, Krätzig WB, Montag U. Sturmbeanspruchte dünne Stahlbetonschalen im Ingenieurbau (Gale-stressed thin RC shells in structural engineering). In: Strack M, Mark P. 25 Jahre in Forschung, Lehre und Praxis, Festschrift Prof. Stangenberg, Ruhr-University Bochum; 2007.
[49] von Backströn TW, Harte R, Höffer R, Krätzig WB, Kröger DG, Niemann HJ, van Zijl GPAG. State and recent advances in research and design of solar chimney power plant technology. VGB PowerTech Journal 2008;(PT07):64–71, July 2008.
[50] Pretorius JP. Solar tower power plant performance characteristics. Master thesis. South Africa: University of Stellenbosch; 2004.
[51] Pretorius JP, Kröger DG. Solar chimney power plant performance. J Solar Energy Eng 2006;128:302–11.
[52] Pretorius JP, Kröger DG. Sensitivity analysis of the operating and technical specifications of a solar chimney power plant. J Solar Energy Eng 2007;129: 171–8.
[53] Hedderwick RA. Performance evaluation of a solar chimney power plant. M.Sc.Eng. thesis. Stellenbosch, South Africa: University of Stellenbosch; 2001.
[54] Bernardes MA dos S. Technische, ökonomische und ökologische Analyse von Aufwindkraftwerken (Technical, economical and ecological analysis of SCPP). Ph.D. Thesis. Germany: Universität Stuttgart; 2004.
[55] Bernardes MA dos S, Voss A, Weinrebe G. Thermal and technical analyzes of solar chimneys. Solar Energy 2003;75:511–24.
[56] Pretorius JP, Kröger DG. Critical evaluation of solar chimney power plant performance. Solar Energy 2006;80:535–44.
[57] Bernardes MA dos S, von Backström TW, Kröger DG. Critical evaluation of heat transfer coefficients applicable to solar chimney power plant collectors. In: Proc. ISES 2007 solar world congress conference; 2007.p. 1706–13.
[58] Bernardes MA dos S, von Backström TW, Kröger DG. Analysis of some available heat transfer coefficients applicable to solar chimney power plant collectors. Solar Energy 2009;83:264–75.
[59] Kröger DG, Buys JD. Solar chimney power plant performance characteristics. S Afr Inst Mech Eng R&D J 2002;15:31–6.
[60] Zhou XP, Yang JK, Wang JB, Xiao B, Hou GX, Wu YY. Numerical investigation of a compressible flow through a solar chimney. Heat Transfer Eng 2009;30:670–6.
[61] Fluent Inc. FLUENT 6 User Guide, Lebanon, New Hampshire; 2001.
[62] AEA Technology. CFX 5.6 User Guide, Harewell, UK; 2003.
[63] Mullett LB. The solar chimney overall efficiency, design and performance. Int J of Ambient Energy 1987;8:35–40.
[64] Lodhi MAK. Application of helio-aero-gravity concept in producing energy and suppressing pollution. Energy Convers Manage 1999;40:407–21.
[65] Pastohr H, Kornadt O, Gurlebeck K. Numerical and analytical calculations of the temperature and flow field in the upwind power plant. Int J Energy Res 2004;28:495–510.
[66] Onyango FN, Ochieng RM. The potential of solar chimney for application in rural areas of developing countries. Fuel 2006;85:2561–6.
[67] Lautenschlaqer H, Haaf W, Schlaich J. New results from the solar chimney prototype and conclusions for large power plants. In: Commission of the European Communities, European. 1985. p. 231–5.
[68] Zhou XP, Yang JK, Xiao B, Hou GX. Simulation of a pilot solar chimney power equipment. Renewable Energy 2007;32:1637–44.
[69] von Backström TW, Gannon AJ. The solar chimney air standard thermodynamic cycle. SAIMechE R&D J 2000;16:16–24.
[70] Hedderwick RA. Performance evaluation of a solar chimney power plant. M.Sc. Eng. thesis. University of Stellenbosch; 2001.
[71] von Backström TW, Fluri TP. Maximum fluid power condition in solar chimney power plants—an analytical approach. Solar Energy 2006;80: 1417–23.
[72] White FM. Fluid mechanics, fifth ed., McGraw-Hill; 2003.
[73] Kolb S, Helmrich T. Strömungstechnische Auslegung eines Aufwindkraftwerks mit 200 MW Leistung (aerodynamic design of a 200 MW solar chimney power plant). Diploma thesis. Institut für Strömungsmechanik und hydraulische Strömungsmaschinen, Universität Stuttgart; 1996 [in German].
[74] Japikse D, Baines NC. Introduction to turbomachinery. Norwich: Concepts ETI, Inc.; 1994.
[75] Idelchik IE. Handbook of hydraulic resistance. Hemisphere Publishing Corporation; 1986.
[76] Kirstein CF, von Backström TW. Flow through a solar chimney power plant collector-to-chimney transition section. J Solar Energy Eng 2006;128:312–7.
[77] Poore R, Lettenmaier T. WindPACT Advanced wind turbine drive train designs study. Tech. Rep. NREL/SR-500-33196. Colorado: National Renewable Energy Laboratory; 2003.
[78] Bywaters G, John V, Lynch J, Mattila P, Norton G, Stowell J, et al. Northern Power Systems WindPACT drive train alternative design study report. Tech. Rep. NREL/SR-500-35524. Colorado: National Renewable Energy Laboratory; revised October, 2004.
[79] Fluri TP, von Backström TW. Performance of the power conversion unit of a solar chimney power plant. In: Proceedings of the 9th World renewable energy congress, conference, Florence, Italy; August 2006.
[80] Zhou XP, Yang JK, Xiao B, Shi XY. Special climate around a commercial solar chimney power plant. ASCE J Energy Eng 2008;134:6–14.
[81] Guo J, Ruan YL. Air pollution control engineering. Beijing, China: Chemical Industry Press; 2001 [in Chinese].
[82] VanReken TM, Nenes A. Cloud formation in the plumes of solar chimney power generation facilities: A modeling study. J Solar Energy Eng 2009;131. 011009-1-10.
[83] Zhou XP, Yang JK, Ochieng RM, Xiao B. Numerical investigation of a plume from a power generating solar chimney in an atmospheric cross flow. Atmos Res 2009;91:26–35.
[84] Zhou XP, Yang JK, Xiao B. Solar power generation and use of grassland in ecology management. In: Schröder HG, editor. Grasslands: ecology, management and restoration. Hauppauge, NY, USA: Nova Science Publishers Inc.; November 1, 2009. ISBN: 9781606920244.
[85] Krisst RJK. Energy transfer system. Alternat Sources Energy 1983;63:8–11.
[86] Kulunk H. A prototype solar convection chimney operated under Izmit conditions. In: Veiroglu TN, editor. Proceedings of the 7th Miami international conference on alternative energy sources; 1985. p. 162.
[87] Pasumarthi N, Sherif SA. Experimental and theoretical performance of a demonstration solar chimney model. Part II: experimental and theoretical results and economic analysis. Int J Energy Res 1998;22:443–61.
[88] Sherif SA, Pasumarthi N, Harker RA, Brinen GH. Performance of a demonstration solar chimney model for power generation. Final Technical Report No. UFME/SEECL-9507, Solar Energy and Energy Conversion Laboratory, Department of Mechanical Engineering, University of Florida, Gainesville, Florida; December, 1995.
[89] Zhou XP, Yang JK. Temperature field of solar collector and application potential of solar chimney power systems in China. J Energy Inst 2008; 81:25–30.
[90] Zhou XP, Yang JK, Xiao B, Hou GX. Experimental study of the temperature field in a solar chimney power setup. Appl Therm Eng 2007;27:2044–50.
[91] Ketlogetswe C, Fiszdon JK, Seabe OO. Solar chimney power generation project—the case for Botswana. Renewable Sustain Energy Rev 2008;12: 2005–12.
[92] Ferreira AG, Maia CB, Cortez MFB, Valle RM. Technical feasibility assessment of a solar chimney for food drying. Solar Energy 2008;82:198–205.
[93] Maia CB, Ferreira AG, Valle RM, Cortez MFB. Theoretical evaluation of the influence of geometric parameters and materials on the behavior of the airflow in a solar chimney. Comput Fluids 2009;38:625–36.
[94] Maia CB, Ferreira AG, Valle RM, Cortez MFB. Analysis of the airflow in a prototype of a solar chimney dryer. Heat Transfer Eng 2009;30:393–9.
[95] Koyun A, Üçgül I, Acar M, Şenol R. Güneş Bacası Sisteminin Termal Özet Dizaynı. Tesisat Mühendisliği Dergisi 2007;98:45-50. available at: http://www.mmoistanbul.org/yayin/tesisat/98/6.
[96] Golder K. Combined solar pond and solar chimney. Final year Mechanical Engineering Project. School of Aerospace, Mechanical and Manufacturing Engineering, Bundoora Campus, RMIT University, Melbourne, Australia; 2003.
[97] Akbarzadeh A, Johnson P, Singh R. Examining potential benefits of combining a chimney with a salinity gradient solar pond for production of power in salt affected areas. Solar Energy 2009;83:1345–59.
[98] Louis T. Optimizing collector efficiency of a solar chimney power plant. IEEE 1985;219–22.
[99] Padki MM, Sherif SA. Solar chimney for medium-to large scale power generation. In: Proceedings of the Manila international symposium on the development and management of energy resources, vol. 1; 1989. p. 432–7.
[100] Padki MM, Sherif SA.In: Solar chimney for power generation in rural areas. Seminar on energy conservation and generation through renewable resources, Ranchi, India. 1989. p. 91–6.
[101] Padki MM, Sherif SA. A mathematical model for solar chimneys. In: Proceedings of 1992 international renewable energy conference, vol. 1; 1992. p. 289–94.
[102] Padki MM, Sherif SA. On a simple analytical model for solar chimneys. Int J Energy Res 1999;23:345–9.
[103] Schlaich J, Schiel W, Friedrich K, Schwarz G, Wehowsky P, Meinecke W, et al.. The solar chimney: transferability of results from the Manzanares solar chimney plant to larger scale-plants. Tech. Rep., Schlaich Bergermann und Partner CEs, Stuttgart; 1995.

[104] Schlaich J, Bergermann R, Schiel W, Weinrebe G. Sustainable electricity generation with solar updraft towers. Struct Eng Int 2004;3.
[105] Bernardes MA, dos S, von Backström TW. Evaluation of operational control strategies applicable to solar chimney power plants. Solar Energy 2010; 84:277–88.
[106] Dai YJ, Huang HB, Wang RZ. Case study of solar chimney power plants in Northwestern regions of China. Renewable Energy 2003;28:1295–304.
[107] Zhou XP, Yang JK, Xiao B, Long F. Numerical study of a solar chimney thermal power setup using turbulent model. J Energy Inst 2008;81:86–91.
[108] Zhou XP, Yang JK, Xiao B, Hou GX, Xing F. Analysis of chimney height for solar chimney power plant. Appl Therm Eng 2009;29:178–85.
[109] Zhou XP, Yang JK, Xiao B, Li J. Night operation of solar chimney power system using solar ponds for heat storage. Int J Global Energy Issues 2009;31:193–207.
[110] Zhou XP, Wang F, Fan J, Ochieng RM. Performance of solar chimney power plant in Qinghai-Tibet Plateau. Renewable and Sustainable Energy Reviews. 2010; corrected proofs, doi:10.1016/j.rser.2010.04.017.
[111] Zhou XP, Yang JK, Xiao B. CFD Simulation study on flow field inside the solar power chimney. J Thermal Power 2006;35:23–6 [in Chinese].
[112] Ninic N. Available energy of the air in solar chimneys and the possibility of its ground-level concentration. Solar Energy 2006;80:804–11.
[113] Nizetic S, Ninic N, Klarin B. Analysis and feasibility of implementing solar chimney power plants in the Mediterranean region. Energy 2008;33:1680–90.
[114] Nizetic S, Klarin B. A simplified analytical approach for evaluation of the optimal ratio of pressure drop across the turbine in solar chimney power plants. Applied Energy 2010;87:587–91.
[115] Ming TZ, Liu W, Xu GL, Xiong YB, Guan XH, Pan Y. Analytical and numerical investigation of the solar chimney Numerical simulation of the solar chimney power plant systems coupled with turbine. Renewable Energy 2008;33:897–905.
[116] Ming TZ, Liu W, Xu GL. Analytical and numerical investigation of the solar chimney power plant systems. Int J Energy Res 2006;30:861–73.
[117] Ming TZ, Liu W, Pan Y, Xu GL. Numerical analysis of flow and heat transfer characteristics in solar chimney power plants with energy storage layer. Energy Convers Manage 2008;49:2872–9.
[118] Ming TZ, Liu W, Pan Y. Numerical analysis of the solar chimney power plant with energy storage layer. In: Proc. ISES 2007 solar world congress conference; 2007.p. 1800–5.
[119] Koonsrisuk A, Chitsomboon T. Dynamic similarity in solar chimney modeling. Solar Energy 2007;81:1439–46.
[120] Koonsrisuk A, Chitsomboon T. Partial geometric similarity for solar chimney power plant modeling. Solar Energy 2009;83:1611–8.
[121] Koonsrisuk A, Chitsomboon T. Accuracy of theoretical models in the prediction of solar chimney performance. Solar Energy 2009;83:1764–71.
[122] Koonsrisuk A, Chitsomboon T. A single dimensionless variable for solar chimney power plant modeling. Solar Energy 2009;83:2136–43.
[123] Koonsrisuk A, Lorente S, Bejan A. Constructal solar chimney configuration. International Journal of Heat and Mass Transfer 2010;53:327–33.
[124] Larbi S, Bouhdjar A, Chergui T. Performance analysis of a solar chimney power plant in the southwestern region of Algeria. Renewable Sustain Energy Rev 2010;14:470–7.
[125] Chergui T, Larbi S, Bouhdjar A. Thermo-hydrodynamic aspect analysis of flows in solar chimney power plants—A case study. Renewable Sustainable Energy Rev 2010;14:1410–8.
[126] Chergui T, Larbi S, Bouhdjar A. Analysis of flows modelling and energy performances in solar chimneys. Int Rev Modell Simul 2008;1:214–20.
[127] Chergui T, Larbi S, Bouhdjar A, Gahgah M. Heat transfer modelling analysis of flows in solar chimneys. In: Proceedings of the fourth international conference on computational heat and mass transfer; 2009.
[128] Petela R. Thermodynamic study of a simplified model of the solar chimney power plant. Solar Energy 2009;83:94–107.
[129] Fluri TP, Pretorius JP, Van Dyk C, von Backström TW, Kröger DG, Van Zijl GPAG. Cost analysis of solar chimney power plants. Solar Energy 2009; 83:246–56.
[130] US Energy Information Administration; 2006.
[131] Greentower. http://www.greentower.net.
[132] Bonnelle D. Private communication; 2008.
[133] Papageorgiou CD. Floating solar chimney. WO2004/085846 A1/07-10-2004.
[134] Papageorgiou CD. Floating solar chimney. http://www.floatingsolarchimney.gr. April 28, 2006.
[135] Papageorgiou CD. Floating solar chimney versus concrete solar chimney power plants. In: Proceedings of international conference on clean electrical power 2007; 2007. p. 760–5.
[136] Papageorgiou CD. Floating solar chimney technology: a solar proposal for China. In: Proc. ISES 2007 solar world congress conference; 2007.p. 172–6.
[137] Papageorgiou CD. Floating solar chimney: the link towards a solar future. In: Proc. ISES 2005 solar world congress conference; August 2005.
[138] Papageorgiou CD. External wind effects on floating solar chimney. In: IASTED proceedings of power and energy systems, EuroPES 2004, conference; July 2004.p. 159–63.
[139] Papageorgiou CD. Optimum design for solar power stations with floating solar chimneys. In: Proceedings of ISES Asia Pacific solar energy conference; October 2004. p. 763–72.
[140] Papageorgiou CD. Turbines and generators for floating solar chimney power stations. In: Proceedings of the IASTED conference on european power and energy systems; June 2006. p. 26–8.
[141] Zhou XP, Yang JK, Wang F, Xiao B. Economic analysis of floating solar chimney power plant. Renewable Sustainable Energy Rev 2009;13:736–49.
[142] Zhou XP, Yang JK. A novel solar thermal power plant with floating chimney stiffened onto a mountain-side and potential of the power generation in China's deserts. Heat Transfer Eng 2009;30:400–7.
[143] Bilgen E, Rheault J. Solar chimney power plants for high latitudes. Solar Energy 2005;79:449–58.
[144] Wei J, Wang FH, Zhao L. Research on the best slope gradient of slope solar induced convective flows power generation system. In: Proc. ISES 2007 solar world congress conference; 2007.p. 1795–9.
[145] Zhou XP, Yang JK, Wang JB, Xiao B. Novel concept for producing energy integrating a solar collector with a man made mountain hollow. Energy Convers Manage 2009;50:847–54.
[146] Kashiwa BA, Kashiwa CB. The solar cyclone: a solar chimney for harvesting atmospheric water. Energy 2008;33:331–9.
[147] Kashiwa BA, Kashiwa CB. The solar cyclone. In: Frangopoulos CA, Rakopoulos CD, Tsatsaronis G, editors. ECOS 2006: Proceedings of the 19th international conference on efficiency, cost, optimization, simulation and environmental impact of energy Systems. Zografou: National Technical University of Athens; 2006. p. 1507–16.
[148] Zhou XP, Yang JK, Wang JB, Xiao B. A novel concept for constructing plant supported a leaning solar chimney power by a mountain. Renewable Energy 2006;(4):9–11 [in Chinese].
[149] Wang YP, Fang ZL, Zhu L, Yang ZY, Wang JH, Han LJ. Study on the integrated utilization of seawater by solar chimney. Acta Energiae Solaris Sinica 2006;27:382–7 [in Chinese].
[150] Wang YP, Wang JH, Zhu L, Yang ZY, Fang ZL. The study of sea desalination and hot wind electric power integrated system by solar chimney. Acta Energiae Solaris Sinica 2006;27:731–6 [in Chinese].
[151] Zhou XP, Xiao B, Liu WC, Guo XJ, Yang JK, Fan Jian. Comparison of classical solar chimney power system and combined solar chimney system for power generation and seawater desalination. Desalination 2010;250:249–56.